MEASUREMENTS OF DRAG COEFFICIENTS FOR FALLING AND RISING SPHERES IN FREE MOTION

Thesis by

A. Werner Preukschat

In Partial Fulfillment of the Requirements

For the Degree of

Aeronautical Engineer

California Institute of Technology

Pasadena, California

1962

ACKNOWLEDGEMENTS

The author wishes to express his deep gratitude to Professor H. W. Liepmann under whose expert guidance the present work was performed and for his advice and the many helpful suggestions, and to Professors Millikan and Zukoski, members of his supervising committee.

The author would also like to acknowledge his indebtedness to Professor Wu for placing the test facilities in the Hydrodynamics Laboratory at the author's disposal.

Thanks are also extended to Mrs. Geraldine Krentler for typing the manuscript and to the staff of the Guggenheim Aeronautical Laboratory and the Hydrodynamics Laboratory for their kind help with the experiments.

The author wishes to express his special gratitude to the executive committee of the Deutscher Akademischer Austauschdienst by whom the author was appointed as NATO Graduate Fellow for the years 1960 to 1962.

ABSTRACT

The purpose of this thesis is to investigate the drag coefficient of spheres in free motion, falling and rising, in water.

Following the introduction the test set-up, sphere release mechanism, spheres and timing device and recorder are described.

Section 3 gives the results of the drag coefficient measurements for free falling spheres which show good agreement with the known measurements, quoted, for instance, in the Handbuch der Experimentalphysik.

Section 4 deals with the measurement of drag coefficients of free-rising spheres. It was found that the freely rising spheres move in an oscillatory path of which wavelength and amplitude depend on the ratio of sphere density and water density.

The local drag coefficient of the spheres was measured to be the same as for falling spheres. It was found to be independent of the sphere motion.

No critical Reynolds number was found for the onset of the oscillatory motion of the sphere. The oscillatory motion appeared to be independent of initial disturbances of the sphere motion.

From photographs of the sphere paths Strouhal numbers were formed which are about one third the value given for circular cylinders in the same Reynolds number range.

A theoretical oscillatory force coefficient, based on a force balance on the sphere, was obtained. It was found to be of the same order of magnitude as the correspondent, actually measured

oscillatory force coefficient on a circular cylinder.

The Strouhal number based on the main theoretical frequency was found to be four times as high as the one calculated from the frequency of the sphere path. It could be, dependent on the sphere density, as high as twice the Strouhal number found for circular cylinders in the same Reynolds number range.

TABLE OF CONTENTS

TABLE OF CONTENTS (Contd.)

LIST OF SYMBOLS

a	radius of sphere
A	amplitude of sphere path
B	buoyant force
C_D	drag coefficient
C_{DH}	drag coefficient, quoted by the Handbuch der Experimentalphysik (1)
C_K	lateral oscillatory force coefficient
d	diameter of sphere
D	diameter of test tube
f	function (Appendix B)
F	inertia force
g	gravitational constant (c.g.s)
h_1	function (Appendix B)
h_2	function (Appendix B)
K	pressure force
K_w	wall correction factor
M	total mass
n	frequency
P	force (Appendix B)
Re	Reynolds number
s	local direction of sphere motion
S	Strouhal number
t	time
T	temperature in degree Celsius

LIST OF SYMBOLS (Contd.)

U	velocity
V	velocity
v	coordinate in v-direction (Appendix B)
W	weight
y	horizontal coordinate of sphere motion
z	vertical coordinate of sphere motion
α	angle of sphere path with vertical z
β	angle (Appendix B)
γ	weight density, gr. wt/cm^3
λ	wavelength of sphere path
υ	kinematic viscosity
ρ	mass density, gr/cm^3

Subscripts

meas	measured
MS	mean square
o	in vertical (z) direction
s	sphere
U	local, in s-direction
v	local, in v-direction
w	water

1. INTRODUCTION

In some experiments made in the Mercury Tank at the Guggenheim Aeronautical Laboratory to determine magneto-fluid dynamic effects on the drag on spheres, it was noticed that the measured drag of freely rising spheres, with no magnetic field, could be as much as twice the "accepted" value, quoted, for instance, by the Handbuch der Experimentalphysik (Ref. 1). The Handbuch values are based on experiments with falling or fixed spheres; and differences in drag for rising and falling spheres have been previously observed by Hesselberg and Birkeland (Ref. 2) and others.

It thus seems that the flow around a rising sphere is somehow different from that around a falling one. The purpose of this thesis is to investigate the reasons for such a difference, particularly in the drag coefficient.

2. EQUIPMENT

2.1. Test Set-Up.

It was decided to make measurements of drag with both rising and falling spheres in water in a set-up geometrically similar to the Mercury Tank. A glass tube of 6-inch nominal diameter was mounted on a table (Fig. 1) and filled with water. Vibrations of the tube were prevented by mounting it on a one inch thick rubber ring.

2.2. Sphere Release Mechanism.

The sphere release mechanism, shown in Figure 2, could be mounted either on top or at the bottom of the test tube. The spheres were to be released by three arms (A) which were activated by means of three electro-magnets with 6-volt-DC coils (B). No accelerations on the spheres due to release forces could be observed in any of the tests.

2.3. Spheres.

In order to vary Reynolds number and density ratios ρ_s/ρ_w different spheres were used.

Table 1 gives data on spheres with ρ_s/ρ_w greater than one, Table 2 on those with ρ_s/ρ_w less than one.

The diameters of the spheres were measured using a micrometer. A mean diameter was found by averaging the diameters of ten spheres. The calculation of the sphere volumes was based on this average diameter. The weight of the spheres was determined using a milligram balance.

As it appeared to be very difficult to buy commercial spheres lighter than water in different diameters, several hollow spheres were made using a Teflon mold (Fig. 3). The molding material was Eccobond.

2.4. Timing Device and Recorder.

Several preliminary velocity measurements were made using as timing devices a stopwatch and a magnetic-type indicator. These, however, gave no satisfactory results so that a third timing device had to be built.

Using the principle that a change in light intensity can be detected by photocells, a phototube timing device was constructed. In this device the sphere crosses a light beam which changes the light intensity at the phototube, thus giving rise to a change in electrical potential at the amplifier tube (Fig. 4). The electric circuit is shown in Figure 4a. In order to obtain a large deflection of the galvanometer of the Visicorder, on which the two time signals were recorded, a Heiland M 40-120 galvanometer connected to a zero-balancing output circuit (also shown in Fig. 4a) was used.

With this timing device spheres of diameters down to 0.25 inch were still detectable when crossing the light beam.

3. DRAG MEASUREMENTS OF FREE-FALLING SPHERES

3.1. General Remarks.

The drag coefficient was computed by assuming that the sphere was moving steadily at its terminal velocity when entering the timing distance. Then

$$C_D = \frac{4}{3}\, d.g.\left(\frac{\rho_s}{\rho_w} - 1\right) K_w^2 \; \frac{1}{U^2} \; ; \; U = \frac{s}{t}$$

Furthermore, the Reynolds number is $Re = \frac{Ud}{\nu_w}$, where ν_w, the kinematic viscosity of water, is a function of temperature and was obtained from reference 3. Figure 5 gives ν_w as a function of temperature.

The water temperature was measured using a -10 to +100 degree Celsius thermometer. Fractions of a degree could be estimated to $\pm$ 0.1° C. The density of the water, ρ_w, has been taken constant at 1 gr/cm^3. The influence of the tube walls on the sphere velocity was taken into account by multiplying the measured velocity by a wall correction factor K_w given by Lunnon (Ref. 4). Figure 6 gives K_w as a function of the ratio of sphere diameter to tube diameter.

The spheres were, of course, released from A (Fig. 1).

3.2. Results.

Using the described photoelectric timing device the drag coefficients of several spheres of densities greater than that of water have been determined. The results are given in Table 3 and Figure 7. The corresponding timing distance is also given in Table 3.

3.3. Discussion of Results.

As can be seen from Figure 7 the drag coefficients for the different spheres scatter up to 10 per cent around their mean values, which agrees fairly well with the respective values of C_{DH}. This scatter has been observed by others, too, as shown in Figure 7.

3.4. Conclusion.

From the results of these measurements it was concluded that the timing device works satisfactorily. Furthermore it showed that the drag coefficient for spheres with density ratios down to $\rho_s/\rho_w = 1.1$ is given by the value of C_{DH}.

Therefore, if there occur any changes in sphere drag coefficients they must do so only when the density of the spheres is less than that of the medium, i.e., for rising spheres.

4. DRAG MEASUREMENTS OF FREE-RISING SPHERES

4.1. General Remarks.

As before the drag coefficient was obtained by evaluating the sphere velocity from a distance-time measurement using the photo-electric timing device. Again, it was assumed that the sphere had reached its steady state velocity when entering the timing distance. This timing distance was varied in order to investigate its influence on the measured velocity.

4.2. Spheres Rising in 6-inch Diameter Tube.

Here the sphere release was mounted at the bottom of the tube (B), and the spheres were introduced through the plastic tube (C) (Fig. 1). Otherwise the tests were run in the same way as before.

4.2.1. Results.

The results of these tests are given in Table 4 and Figure 8. It was observed that the spheres rose in an oscillatory motion for which amplitude and wavelength differed from sphere to sphere. Several runs were made without using the sphere release, letting the sphere rise freely out of the plastic tube. No significant change in the behavior of the spheres or in their drag coefficients could be observed.

4.2.2. Discussion of Results.

The oscillatory motion of the rising spheres seems to be a typical feature of the sphere motion. The wavy motion becomes more significant as the density ratio ρ_s/ρ_w decreases. This wavy motion seems to be independent of even large lateral disturbances given initially to the sphere, as in the case where the spheres rose freely through the plastic tube.

The displacement of the sphere out of its straight vertical path can be attributed to a low mass to force ratio, where the force results from non symmetric vortex shedding from the sphere. For a falling sphere the mass to force ratio is greater than that for a rising sphere, so one would expect less significant or no oscillatory motion of the heavy sphere. This was actually observed: the falling spheres moved in a straight path. From the oscillatory sphere motion it can be concluded that the point at which the force acts oscillates geometrically over the sphere. It was furthermore observed that the sphere traveled first along a two-dimensional, wavy path which later changed often into a more or less helical path. No evident reason for this change of motion could be observed. Once in a helical motion, the sphere would never go back into the two-dimensional motion. It sometimes happened, however, that the change from two-dimensional to helical motion did not occur at all, and the sphere traveled only along a sinusoidal path.

The drag coefficient for each sphere shows more or less scatter in a random fashion around a mean value which is higher

than C_{DH}. The drag coefficient of the spheres with density ratios $\rho_s/\rho_w = 0.93$ approach C_{DH} independently of Reynolds number, with the simultaneous disappearance of the oscillatory motion.

The drag coefficients of the spheres with diameter $d = 0.725$ inch and $\rho_s/\rho_w \sim 0.59$ were extensively examined. The scatter of C_D is particularly high for $s = 2$ inch, but is much less for $s = 24$ inch. Furthermore, the lowest values of C_D approach C_{DH}. This suggests that the "local drag coefficient" of the sphere might not be significantly different from the correspondent value of C_{DH} which would have been measured for a falling sphere with same diameter at the same Reynolds number.

Hence, it was assumed that the "apparent drag coefficient" which was actually measured by our method, is the local drag coefficient multiplied by a factor which depends mainly on the location of the wavy sphere path with respect to the timing distance (Fig. 9), and that the local drag coefficient would have been obtained with the sphere velocity $U = ds/dt$.

Considering a sinusoidal sphere path, the ratio of $C_{D,\,max}/C_{D,\,min}$ is equal to $1/\cos^3 \alpha_{max}$ (Appendix A). The calculation was based upon the assumption of a steady state motion along the sinusoidal path. If we take $C_{D,\,min}$ as the value of C_{DH} and $C_{D,\,max}$ as the maximum apparent drag coefficient measured, we find the maximum angle between vertical and sphere path is about 30^o. This is a value which seemed not to be too high compared with the observed motion. Furthermore, a calculated mean square average C_D based on this α_{max} showed good agreement with the average value of C_D obtained for $s = 24$ inch.

4.2.3. Conclusion.

In order to test our assumption, that the local drag coefficient of free-rising spheres in the considered density range is independent of the wavy motion of the sphere and is equal to C_{DH}, it was decided to repeat the tests in the large water tank of the Hydrodynamics Laboratory. The tank was large enough so that the spheres could rise without any wall effects, excluding thus a possible influence of the wall on the motion of the sphere.

4.3. Spheres Rising in Large Water Tank.

The experiments were performed in the water tank of the Hydrodynamics Laboratory. The sphere release mechanism was mounted on a platform and, with the spheres enclosed, lowered to the bottom of the tank, from which the spheres were released one at a time. The temperature of the water was measured as before by a -10 to +100 degree Celsius thermometer.

4.3.1. General Remarks.

The drag coefficients of the spheres with density ratios less than one were evaluated by measuring the local velocity of the spheres with the aid of a Voightländer Bessamatic camera, of which the used shutter time was measured. The shutter time measurements were made by using the photoelectric timing device (Fig. 4), with a light beam which was first sent through the camera. The measured shutter time was 0.190 ± 0.002 sec.

The spheres were photographed when passing a certain point in the water through a window situated at the side of the tank below the water surface, leaving thus a streak on the film corresponding to the traveled distance during the shutter opening. A mirror was placed in the water at an angle of 45° with respect to the camera-sphere plane in order to obtain the three-dimensional path of the sphere.

Other pictures were taken photographing a large part of the sphere path. Motion pictures showing the lateral displacement of the spheres with respect to the vertical axis during its rise were also taken.

4.3.2. Results.

Figure 10 shows the reproduction of one of the pictures (sphere No. 47) from which the local sphere velocities were determined which are given in Table 5. Figures 11 to 14 give reproductions of the photographs of the different sphere paths, Figures 15 and 16 reproductions of the lateral displacements of the spheres.

Table 5 gives also the drag coefficients obtained during these tests; these are plotted on Figure 8.

Table 6 gives the minimum, maximum and average wavelength of the motion of the different spheres; these are non dimensionalized with the sphere diameter and plotted in Figure 17 versus the density ratio. In Table 7 the maximum lateral amplitudes of the sphere path are given and plotted in Figure 18; they are determined either from the sphere path pictures of the Figures 11 to 14 or from the Figures 15 and 16.

4.3.3. Discussion of Results.

The experiments carried out in the water tank show that the local drag coefficients of the rising spheres, for the densities considered, are indeed those given by the values of C_{DH}, within the usual scatter observed for sphere drag coefficients. This is true independently of the oscillatory motion with which the sphere rises.

A distinct wavelength of the sphere motion is observed, which is constant along the sphere path within an average maximum scatter of 11.41 per cent of all spheres (Table 6). The two-dimensionality of the photographs has here no effect on the measurement.

The evaluation of the lateral amplitudes of the sphere motion has been carried out, but it could not be done very accurately because of either the two-dimensionality of the Figures 11 to 14 or of the changing scale of the Figures 15 and 16; this may account for the large scatter of data in Figure 18. The sphere sometimes experiences sudden displacements from its general axis of motion, for which no obvious reason could be observed.

It was again observed that the sphere traveled first in a two-dimensional motion which went over later into a helical motion. This was especially well seen for sphere No. 39 (Fig. 16). It was however noticed that the sphere did not remain during all its rise in this two-dimensional motion, as it sometimes did in the experiments in the 6-inch diameter tube.

The oscillatory motion of the spheres died out when the density ratio ρ_s/ρ_w approached one and their drag coefficients became C_{DH}

independently of the timing distance. This was observed to be true independently of Reynolds number, too (Fig. 8, spheres No. 31 and 38), which indicates that there is no critical Reynolds number for the onset of significant oscillations of the rigid spheres.

As it has been observed by Winny (Ref. 5) there exists a typical vortex shedding from a sphere in the Reynolds number range considered. He observed furthermore that the average vortex frequency on the surface of the sphere is not the same as in the wake but is about four times higher. Due to this vortex motion, superimposed on the straight fluid motion, the fluid will exert additional fluctuating pressure on the sphere which will influence the sphere path if the inertia of the sphere is not too high.

Therefore the motion of the sphere will be determined primarily by the sphere mass and the sphere will respond significantly only to the lowest frequencies with the highest energy. As Fung (Ref. 6) has shown the maximum of the power spectrum occurs at a Strouhal number $S = \frac{nd}{U_o}$ which is quite low and almost constant at $S = 0.05$ for Reynolds numbers from 0.33×10^6 to 1.27×10^6. Assuming this to be true for lower Reynolds numbers, too, this would explain the low Strouhal numbers obtained from the photographs, given in Figure 19, in comparison with those observed for cylinders in the same Reynolds number range, cf. A. Roshko (Ref. 7), who gives $S = 0.21$.

As it is quite difficult to obtain much detailed information about the fluctuating pressure distribution over the sphere during its rise an attempt has been made to obtain an expression for the time

varying pressure force (i.e., the pressure integral over the sphere) by considering the force balance on the sphere under some simplifying assumptions.

In Appendix B the necessary pressure integral which must balance the buoyant force and the inertia force has been calculated under the following assumptions:

1. The drag of the sphere is equal to the buoyant force times the cosine of the sphere path angle with the vertical,
2. the sphere path is sinusoidal and two-dimensional,
3. the velocity is constant in vertical direction.

The calculations give a time dependent lateral force K which is given in Figure 20 as a function of α or time. For sphere No. 47, for which an example has been calculated through, the maximum force is $K_{max} = 1.44$ gr. wt. This corresponds to a maximum force coefficient of $C_{max} = 0.16$, which corresponds to a force coefficient for a circular cylinder of $C_{max, cyl.} = 0.786$. This is of the same order of magnitude as H. Drescher (Ref. 8) has actually measured for circular cylinders in water at $Re = 1.13 \times 10^5$, as he obtains oscillating force coefficients between 0.6 and 1.3.

Hence, although the approximation is quite crude, it gives reasonable results for the maximum force coefficient of the sphere in connection with the observed data for the sphere path.

In Figure 21 the force coefficient is given over one wavelength of the sphere path. Due to the interaction of buoyant force and inertia force a whole frequency spectrum for the resultant pressure force is

created in which mainly the frequencies 2f and 4f appear, where f is the frequency of the sphere motion. As the amplitudes of the 4f-force are much higher than any other, the theoretical force coefficient would therefore give a four times higher Strouhal number, which would correspond to the observations Winny (Ref. 5) has made. Hence, based on the calculations of the necessary force coefficient, a theoretical Strouhal number is found with a value between 0.1496 and 0.354 depending on the density ratio ρ_s/ρ_w.

The fact that the Strouhal number seems to be a function of ρ_s/ρ_w is due to the method of determining the Strouhal number, i.e., by evaluating S from the response of the sphere to a certain oscillatory force. As the ratio ρ_s/ρ_w decreases the sphere will respond more to higher frequencies and therefore the Strouhal number, formed with the observed data will increase. For fixed bodies, on which the reference Strouhal number measurements have been performed, there is, of course, no influence due to a change in density of the body.

4.3.4. Summary.

The drag coefficients of rigid, freely rising spheres in water with densities in the range $0.526 < \rho_s < 0.93$ gr/cm^3 were found to be the same as those for rigid, free-falling spheres of densities larger than one gr/cm^3 with the same diameter, at the same Reynolds number.

The drag coefficients were found to be independent of the oscillatory sphere motion which dies out when the density ratio ρ_s/ρ_w approaches one. This oscillatory motion was practically non-existent for $\rho_s/\rho_w = 0.93$ independently of the Reynolds number, so that a critical Reynolds number for the oscillations of the sphere path could not be found.

"Apparent drag coefficients" were obtained when the drag coefficient of the sphere was tried to be determined by a distance per time measurement of the sphere velocity. This apparent drag coefficient was found to be a function only of the geometry of the sphere path along which the sphere traveled.

The oscillatory motion of the sphere was first a two-dimensional motion, then changed sometimes into a helical one, for which no reason could be observed.

For both the two-dimensional and the helical motion a distinct wavelength could be found which remains constant along the sphere path within a certain amount of scatter. The amplitudes of the sphere motion are given only approximately.

From photographic pictures of the sphere path Strouhal numbers

have been found which depend on the sphere densities and are about three times smaller than those obtained for oscillating flow over circular cylinders.

Under certain simplifying assumptions the necessary pressure force for a force balance on the sphere has been calculated. This gives a maximum force coefficient of the same order of magnitude as observed for fluctuating force coefficients on circular cylinders.

The theoretical pressure force fluctuates with a main frequency which is four times larger than the sphere path frequency giving rise thus to a theoretical Strouhal number range around the value measured for circular cylinders.

References

1. Handbuch der Experimentalphysik, Band 4, 2. Teil (1932).

2. Th. Hesselberg und B. J. Birkeland: Steiggeschwindigkeit der Pilotballone, Beitr. z. Phys. d. freien Atmosph., 4, 196 (1912).

3. O. W. Eshbach: Handbook of Engineering Fundamentals, Vol. 1 (1936).

4. R. G. Lunnon: Fluid Resistance to Moving Spheres, Proc. Roy. Soc. London (A) 118, 680 (1928).

5. H. F. Winny: Vortex System Behind a Sphere Moving Through Viscous Fluid, A. R. C. Reports and Memoranda No. 1531, T. 3305 (1932).

6. Y. C. Fung: Fluctuating Lift and Drag Acting on a Cylinder in a Flow at Supercritical Reynolds Numbers. IAS-Paper No. 60-6 (1960).

7. A. Roshko: On the Development of Turbulent Wakes from Vortex Streets, Thesis, California Institute of Technology, (1952).

8. H. Drescher: Messung der auf querangeströmte Zylinder ausgeübten zeitlich veränderlichen Drücke, Z. f. Flugwiss. 4, Heft 1/2, pp. 17-21 (1956).

APPENDIX A

CALCULATION OF SPHERE DRAG COEFFICIENT.

Assumptions :

1. DRAG OF SPHERE $D = B_o \cos\alpha$

where $B_o = g\rho_w \frac{4}{3}\pi a^3 \left(1 - \frac{\gamma_s}{\gamma_w}\right)$

$D = C_D \frac{1}{2} \rho_w U^2 \pi a^2$

2. SPHERE PATH $y = A \cos \frac{2\pi z}{\lambda}$

3. In vertical direction $z = U_o t$ $U_o = \text{const.}$

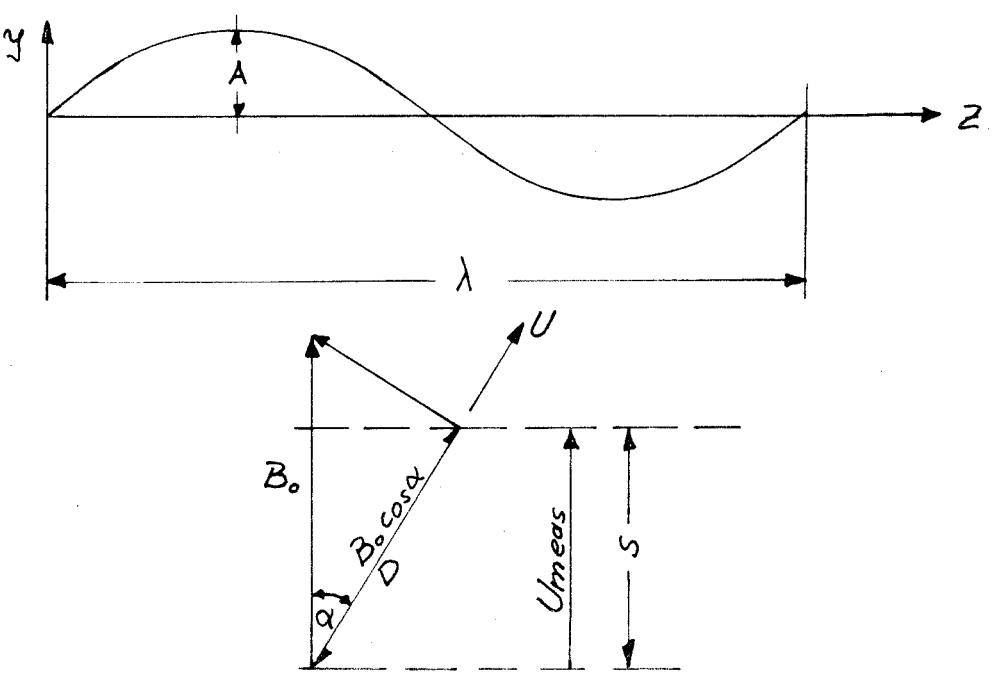

measured velocity $U_{meas} = \frac{s}{t}$

local velocity $U = \frac{1}{\cos\alpha} U_{meas}$

From $B_o \cos\alpha = D$

$$C_{D,U} = \frac{g \frac{4}{3} d \left(1 - \frac{\gamma_s}{\gamma_w}\right) K_w^2}{U^2} \cos\alpha$$

$$= \frac{g \frac{4}{3} d \left(1 - \frac{\gamma_s}{\gamma_w}\right) K_w^2}{U_{meas}^2} \cos^3\alpha$$

or

$$C_{D,U} = C_{D,meas} \cdot \cos^3\alpha$$

Mean square drag coefficient:

$$U_{MS} = \left\{ \frac{1}{L} \int_0^L U_o^2 \left[1 + (tg\,\alpha_{max})^2 \cos^2 \frac{2\pi z}{\lambda} \right] dz \right\}^{1/2}$$

Hence, with U_o = constant

$$\frac{C_{D,MS}}{C_{D,meas}} = \frac{U_{meas}^2}{U_{MS}^2} = \frac{U_{meas}^2}{U_o^2 \left(1 + \frac{1}{2} tg^2 \alpha_{max}\right)}$$

From assumption 1 : $U = U_0 \sqrt{\cos\alpha}$

and $U_{meas} = U \cos\alpha$

Hence :

$$\frac{C_{D,MS}}{C_{D,U}} = \frac{1}{1 + \frac{1}{2} tg^2 \alpha_{max.}}$$

EXAMPLE :

Sphere No. 48 to 58 :

$d = 0.725$ in ; $S = 1.95$ inch

Assuming $C_{D,U} \equiv C_{DH} = 0.403$

With $C_{D,meas,max} = 0.619$

$$\frac{C_{DH}}{C_{D,meas,max.}} = \cos^3 \alpha_{max} = 0.652$$

$$\alpha_{max} = 29.8°$$

and $C_{D,MS} = 0.470$

$C_{D,MS}$ is plotted on figure 8.

APPENDIX B

CALCULATION OF FORCES ON SPHERE.

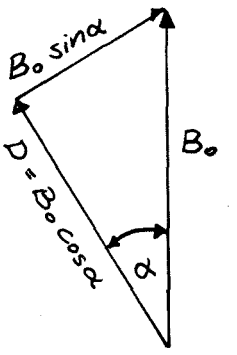

Assumptions :

1. Drag of sphere $D = B_o \cos\alpha$

where $B_o = g\,\rho_w \frac{4}{3}\pi a^3 \left(1 - \frac{\gamma_s}{\gamma_w}\right)$

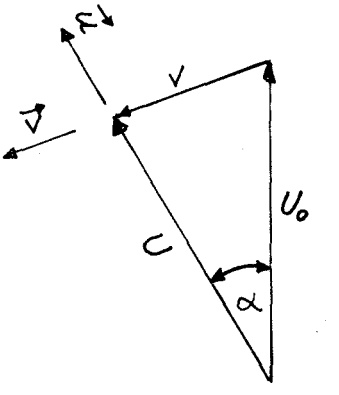

2. Sphere path $y = A\cos\frac{2\pi z}{\lambda}$

3. In vertical direction $z = U_o t$

U_o = const.

Force balance :

From 1. : $U^2 C_D \frac{1}{2} \rho_w 4\pi a^2 = D = B_o \cos\alpha$

$$U = U_o \sqrt{\cos\alpha}$$

where $$U_o^2 = \frac{2B_o}{C_D \rho_w 4\pi a^2} = \frac{2ga(1 - \frac{\gamma_s}{\gamma_w})}{3 C_D}$$

A. Force Balance in U - direction:

$$\text{Drag} + \text{Inertia force} = B_o \cos\alpha + \text{Pressure force})_u$$

$$\text{with 1.} \qquad M \frac{dU}{dt} \equiv F_U = P_U$$

where M = Mass of sphere + Apparent mass.

$$M = \frac{4}{3}\pi a^3 \rho_w \left(\frac{1}{2} + \frac{\gamma_s}{\gamma_w} \right)$$

with $U = U_o \sqrt{\cos\alpha}$; $\operatorname{tg}\alpha = -\frac{2\pi A}{\lambda} \sin\frac{2\pi z}{\lambda}$; $z = U_o t$

we have $$\frac{d\alpha}{dt} = -\frac{4\pi^2 A}{\lambda^2} U_o \cos\frac{2\pi z}{\lambda} \cos^2\alpha$$

$$\frac{dU}{dt} = \frac{U_o^2}{\sqrt{\cos\alpha}} \frac{2\pi^2 A}{\lambda^2} \cos\frac{2\pi z}{\lambda} \cos^2\alpha \sin\alpha$$

and

$$F_U = M U_o^2 \frac{2\pi^2 A}{\lambda^2} \cos\frac{2\pi z}{\lambda} \cos^{3/2}\alpha \sin\alpha \equiv f \cdot h_1(\alpha)$$

$$f \equiv M U_o^2 \frac{2\pi^2 A}{\lambda^2} \cos\frac{2\pi z}{\lambda}$$

B. Force Balance in V-direction:

$$\text{Inertia force} + B_o \sin\alpha = \text{Pressure force}\Big|_V$$

$$M \frac{dV}{dt} \equiv F_V$$

$$V = U_o \left[1 + \cos\alpha - 2\cos^{3/2}\alpha \right]^{1/2}$$

$$F_V = -MU_o^2 \frac{2\bar{\imath}^2 A}{\lambda^2} \cos\frac{2\bar{\imath}z}{\lambda} \frac{(3\cos^{1/2}\alpha - 1)\cos^2\alpha}{\left[1 + \cos\alpha - 2\cos^{3/2}\alpha\right]^{1/2}} \sin\alpha$$

$$\equiv -f\, h_2(\alpha) \quad ; \quad \lim_{\alpha \to o} h_2(\alpha) = 2$$

From the figure below we obtain the force P which exerts the sphere on the fluid from geometrical considerations. P must be balanced by a pressure force K which exerts the fluid on the sphere.

We obtain:

$$F_1 = F_U \cos\alpha + F_V \cos\beta$$

$$F_2 = F_v \sin\beta - F_u \sin\alpha$$

$$F^2 = F_1^2 + F_2^2$$

$$P_1 = K_1 = B \sin\alpha + F_1$$

where $B = B_o \sin\alpha$

$$P_2 = K_2 = B \cos\alpha + F_2$$

$$K^2 = K_1^2 + K_2^2$$

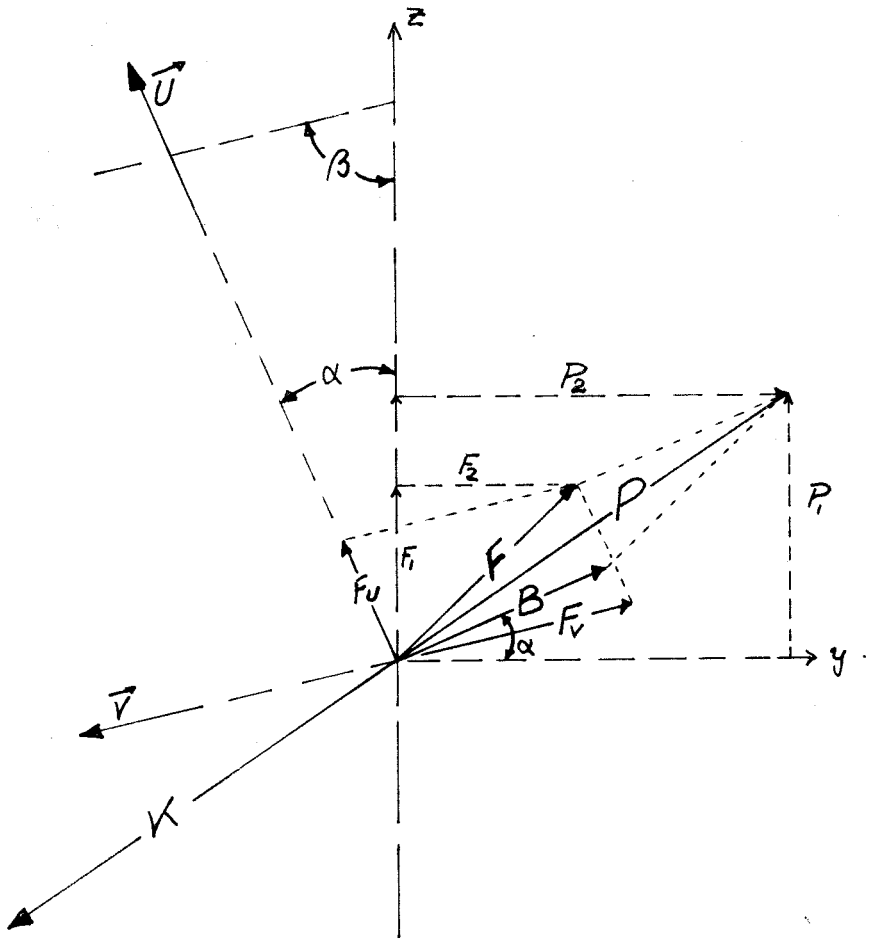

We get:

$$F^2 = F_U^2 + F_V^2 + 2 F_U F_V \cos(\alpha+\beta)$$

and $$K^2 = B^2 + F_U^2 + F_V^2 + 2 F_U F_V \cos(\alpha+\beta) + 2 B F_V \sin(\alpha+\beta)$$

with $$B_o^2 \sin^2\alpha = B^2 = D_o^2 \sin^2\alpha$$

where $$D_o = c_D \tfrac{1}{2} \varrho_w 4\pi a^2 U_o^2$$

and $$F_U = f\, h_1(\alpha) \quad ; \quad F_V = -f\, h_2(\alpha)$$

We obtain finally the <u>necessary pressure force</u> K:

$$K = \left\{ \left[c_D \varrho_w 2\pi a^2 U_o^2 \sin\alpha \right]^2 + f^2 \left[h_1^2 + h_2^2 - 2 h_1 h_2 \cos(\alpha+\beta) \right] + \right.$$

$$\left. - c_D \varrho_w 4\pi a^2 U_o^2 \sin\alpha \cdot f \cdot h_2 \cdot \sin(\alpha+\beta) \right\}^{1/2}$$

$$f = \frac{8}{3} \pi^3 a^3 \frac{1}{g} \gamma_w \left(0.5 + \frac{\gamma_s}{\gamma_w}\right) U_o^2 \frac{A}{\lambda^2} \cos\frac{2\pi z}{\lambda}$$

$$h_1 = \cos^{3/2}\alpha \cdot \sin\alpha$$

$$h_2 = \left(3\cos^{1/2}\alpha - 1\right)\left[1 + \cos\alpha - 2\cos^{3/2}\alpha\right]^{-\frac{1}{2}} \cos^2\alpha \sin\alpha$$

EXAMPLE: Sphere No. 47.

$\gamma_s/\gamma_w = 0.526$ $\quad a = 0.288$ in $\hat{=}$ 0.782 cm

From photograph: $U_o = 18.9$ in/sec $\hat{=}$ 48 cm/sec

$A = 1.0$ in $\hat{=}$ 2.54 cm

$\lambda = 14.15$ in $\hat{=}$ 35.95 cm

From $tg\,\alpha_{max} = \frac{2\pi A}{\lambda}$: $\alpha_{max} = 23.92°$

We obtain then: (β has been evaluated graphically):

$\alpha°$	0	2.5	5	8	10	15	20	α_{max}
K_{gr}	.783	.61	.455	.2805	.08	.78	.876	1.44
C_K	.087	.0628	.05055	.0312	.00889	.0866	.0974	.16

$K = K(\alpha)$ is given in Figure 20.

$C_K = C_K(\alpha)$ is given in Figure 21.

TABLE 1

Sphere No.	d	W	ρ_s/ρ_w	K_w	$C_D U^2$
	in	gr	-	-	in^2/sec^2
1	0.727	4.282	1.30	0.972	106.02
2	0.650	3.120	1.326	0.975	103.70
3	0.410	0.800	1.354	0.984	72.36
4	0.376	0.5274	1.156	0.9855	29.34
5	0.371	0.976	2.225	0.9857	227.12
6	0.376	1.685	3.72	0.9855	509.72
7	0.300	0.294	1.27	0.9885	40.61
8	0.236	1.530	1.366	0.991	43.64
9	0.750	28.134	7.77	0.971	2464.2
10	0.5935	13.95	7.78	0.977	1977.8
11	0.485	7.603	7.78	0.981	1627.9
12	0.406	4.47	7.78	0.984	1366.9
13	0.250	1.03	7.69	0.99	843.52
14	0.7335	4.43	1.308	0.9715	109.78
15	0.613	2.585	1.31	0.977	93.41
16	0.546	1.842	1.325	0.979	87.49
17	0.487	1.313	1.326	0.981	78.59
18	0.425	0.659	1.320	0.983	67.63
19	0.365	0.416	1.35	0.986	63.56
20	0.75	4.161	1.152	0.971	55.33
21	0.625	2.09	1.156	0.976	47.50
22	0.562	1.518	1.154	0.978	42.56

T A B L E 1 (CONTINUED)

Sphere No.	d in	W gr	ρ_s/ρ_w -	K_w -	$C_D U^2$ in^2/sec^2
23	0.500	1.2344	1.154	0.981	37.88
24	0.437	0.8242	1.161	0.983	35.00
25	0.374	0.5195	1.160	0.986	29.80
26	0.251	0.1564	1.150	0.990	18.99
27	0.218	0.1029	1.160	0.992	17.60
28	0.156	0.3787	1.165	0.995	13.07
29	0.3125	0.3018	1.151	0.988	23.73
30	0.281	0.2206	1.161	0.990	22.80

T A B L E 2

Sphere No.	d	W	ρ_s/ρ_w	K_w	$C_D U^2$	
	in	gr	-	-	in^2/sec^2	
31	0.747	3.343	0.953	0.972	24.34	
32	0.620	1.9015	0.9275	0.977	22.13	
33	0.5625	1.427	0.953	0.979	18.58	
34	0.493	0.9489	0.923	0.981	18.78	
35	0.429	0.6275	0.927	0.983	15.54	
36	0.372	0.4058	0.919	0.986	14.98	
37	0.313	0.2436	0.926	0.988	11.63	
38	0.250	0.1249	0.932	0.990	8.57	
39	0.757	2.3008	0.618	0.9705	140.24	
40	0.755	2.1482	0.582	0.9705	153.11	
41	0.629	1.633	0.7655	0.975	72.05	mold
42	0.637	1.7065	0.770	0.975	71.60	"
43	0.642	1.737	0.765	0.975	73.80	"
44	0.385	0.360	0.735	0.9855	51.00	"
45	0.453	0.546	0.6845	0.9825	71.02	"
46	0.517	1.038	0.875	0.980	31.91	"
47	0.576	0.863	0.526	0.9779	134.33	"
48	0.725	1.922	0.5875	0.972	145.44	
49	"	1.908	0.584	"	146.68	
50	"	1.917	0.586	"	145.96	
51	"	1.917	0.586	"	145.96	
52	"	1.930	0.590	"	144.57	

T A B L E 2 (CONTINUED)

Sphere No.	d	W	ρ_s/ρ_w	K_w	$C_D U^2$
	in	gr	-	-	in^2/sec^2
53	0.725	1.956	0.598	0.972	141.79
54	"	1.917	0.586	"	145.96
55	"	1.930	0.590	"	144.57
56	"	1.952	0.597	"	142.10
57	"	1.908	0.584	"	146.68
58	"	1.940	0.594	"	143.18

TABLE 3

Sphere No. s=12 inch		t sec	U in/sec	C_D -	T ^oC	Re -
1		0.768	15.62	0.435	26.2	8510
2		0.745	16.105	0.400		7840
3		0.89	13.48	0.398		4140
4		1.395	8.6	0.397		2430
5		0.502	23.90	0.398	22.7	6110
		0.51				
		0.528	22.72	0.44		5810
6		0.333	36.35	0.386	26.2	10210
7		1.195	10.04	0.403		2260
8		1.19	10.09	0.429		1780
9		0.159	75.50	0.432	26.0	42250
		0.160				
		0.161				
	3x	0.162				
		0.163	73.60	0.455		41200
10		0.176	68.20	0.425		30200
11		0.193	62.18	0.421		22550
		0.195	61.55	0.430		22200
12	3x	0.206	58.27	0.403		17720
		0.21	57.15	0.419		17410
13		0.253	47.43	0.375		8860
	6x	0.2577	46.70	0.387		8730

T A B L E 3 (CONTINUED)

Sphere No. s=12 inch		t sec	U in/sec	C_D -	T ^oC	Re -
14		0.720	16.66	0.396	26.0	9100
	2x	0.730				
		0.735				
		0.740				
	3x	0.75	16.00	0.429		8730
15		0.77	15.59	0.384	26.0	7120
	2x	0.78				
		0.785				
	3x	0.79				
		0.80				
		0.81				
		0.82	14.63	0.436		6710
16	5x	0.80	15.00	0.389	26.0	6100
	2x	0.82				
		0.825	14.54	0.414		5910
17		0.835	14.38	0.380	26.0	5210
		0.84				
		0.845				
	2x	0.85				
		0.855				
	3x	0.86				
		0.88	13.62	0.424		4950

T A B L E 3 (CONTINUED)

Sphere No.		t	$\bar{U}$	C_D	T	Re
s=12 inch		sec	in/sec	-	°C	-
18	3x	0.895	13.41	0.376	26.0	4260
	2x	0.905				
	4x	0.91				
		0.92	13.04	0.398		4140
19	3x	0.96	12.50	0.407	26.0	3400
	2x	0.965				
		0.97				
		0.975				
		0.980	12.24	0.424		3330
20	3x	1.02	11.77	0.399	26.0	6580
	3x	1.025				
		1.03	11.64	0.408		6520
21		1.07	11.21	0.378	26.0	5230
		1.08				
		1.09				
	3x	1.10				
		1.11				
		1.13				
		1.135	10.58	0.424		4930
22		1.13	10.61	0.378	26.0	4460
	4x	1.15				
	2x	1.16				

T A B L E 3 (CONTINUED)

Sphere No. s=12 inch		t sec	U in/sec	C_D -	T °C	Re -
23		1.19	10.09	0.372	26.0	3760
	2x	1.21				
	4x	1.22				
		1.225				
		1.23				
		1.24	9.68	0.404		3610
24	6x	1.30	9.235	0.410	26.0	3010
	3x	1.31				
		1.315	9.13	0.419		2980
25		1.40	8.58	0.405	26.0	2380
	6x	1.42				
	3x	1.43	8.396	0.423		2340
26	3x	1.79	6.705	0.423	26.1	1262
	5x	1.80				
		1.81	6.635	0.431		1247
27	5x	1.95	6.155	0.416	26.1	1001
	4x	1.96				
		1.97	6.09	0.425		991
28	2x	2.50	4.80	0.568	26.1	559
	2x	2.51				
	2x	2.52				
		2.57	4.17	0.752		486

T A B L E 3 (CONTINUED)

Sphere No. s=12 inch		t sec	U in/sec	C_D -	T °C	Re -
29	2x	1.55	7.745	0.396	22.5	1810
	5x	1.56				
		1.57				
		1.575	7.61	0.410		1780
30	4x	1.65	7.27	0.431	22.5	1405
	2x	1.66				
		1.665				
		1.67				
		1.675				
		1.68	7.145	0.447		1380

T A B L E 4

Sphere No. s=12 inch		t sec	U in/sec	C_D -	T °C	Re -
31		1.47	8.16	0.366	26.1	4540
		1.51				
		1.55				
		1.57	7.645	0.416		4260
32	2x	1.61	7.455	0.398	26.1	3370
		1.64	7.315	0.4135		3320
33	2x	1.72	6.98	0.381	26.1	2940
		1.77				
		1.81	6.635	0.422		2800
34		1.68	7.145	0.368	26.1	2630
		1.72				
		1.76				
		1.77				
	2x	1.78				
	2x	1.79	6.705	0.418		2470
35		1.85	6.485	0.370	26.1	2085
		1.86				
		1.87				
		1.88	6.38	0.382		2045
36		1.96	6.122	0.399	26.1	1705
		1.97				
		1.98				

T A B L E 4 (CONTINUED)

Sphere No. s=12 inch		t sec	U in/sec	C_D -	T °C	Re -
		1.99				
		2.02				
		2.03				
		2.06	5.83	0.426		1620
37	2x	2.29	5.42	0.424	22.6	1226
		2.31				
	2x	2.32				
	2x	2.33				
		2.34	5.13	0.442		1201
38		2.64	4.545	0.415	22.6	850
		2.68				
		2.685				
		2.69				
	2x	2.70				
		2.71				
		2.72				
		2.77	4.33	0.457		810
39		0.761	15.85	0.558	22.7	8270
		0.772				
		0.783	15.31	0.598		7990
40		0.682	17.59	0.495	22.7	9130
		0.705				

T A B L E 4 (CONTINUED)

Sphere No.	t	U	C_D	T	Re
s=12 inch	sec	in/sec	-	°C	-
	0.710				
	0.744	16.13	0.588		8390
41	0.99	12.11	0.491	23.0	5260
2x	1.00				
2x	1.03				
s=24 inch					
	1.98				
	2.00				
	2.01				
	2.10	11.42	0.553		4980
42					
s=12 inch	0.94	12.77	0.439	23.0	5620
	0.93				
	0.92				
s=24 inch					
	1.87				
	1.84				
	1.82	13.19	0.412		5810
43					
s=12 inch	0.90	13.32	0.416	23.0	5940
	0.91				
	0.94				

T A B L E 4 (CONTINUED)

Sphere No.	t	U	C_D	T	Re
	sec	in/sec	-	°C	-
43					
s=24 inch	1.80				
2x	1.84				
	1.87				
	1.88	12.77	0.452		5690
44					
s=24 inch	2.56	9.83	0.58	20.0	2320
	2.57				
	2.59				
	2.61	9.20	0.603		2280
45					
s=24 inch	1.89	12.70	0.440	20.0	3710
	1.90				
	1.91	12.57	0.449		3660
46					
s=24 inch	2.86	8.40	0.453	20.0	2790
	2.90				
	2.93				
	2.94	8.16	0.479		2710
47					
s=24 inch	1.44	16.68	0.483	20.0	6190
	1.47				

T A B L E 4 (CONTINUED)

Sphere No.	t	U	C_D	T	Re
	sec	in/sec	-	°C	-
	1.48				
	1.52				
	1.54	15.59	0.553		5790
s=1.95 inch*					
49	0.11			23.0	
	0.123				
	0.115				
51	0.12				
	0.112				
	0.128	15.23	0.629		7910
52	0.112				
	0.123				
53	0.113				
	0.121				
54	0.113				
	0.111				
55	0.124				
	0.115				
56	0.120				
57	0.108				
58	0.106	18.40	0.426		9410

* without sphere release mechanism

TABLE 4 (CONTINUED)

Sphere No.		t	U	C_D	T	Re
		sec	in/sec	-	°C	-
s=2.0 inch						
48		0.113			22.0	
49		0.130	15.39	0.619		7530
50		0.122				
52		0.118				
53		0.110	18.18	0.429		8900
54		0.113				
56		0.125				
57		0.118				
58		0.111				
s=24 inch						
48	2x	1.40			17.2	
49		1.38				
		1.40				
50		1.37				
	2x	1.35	17.98	0.451		7780
51	2x	1.39				
		1.38				
52		1.39				
		1.40				
		1.41				

T A B L E 4 (CONTINUED)

Sphere No.		t	U	C_D	T	Re
		sec	in/sec	-	°C	-
53		1.405				
		1.39				
54		1.40				
		1.41	17 .02	0.504		7380
56	3x	1.39				
57		1.39				
		1.405				
58		1.39				
		1.41				

TABLE 5

Sphere No.	d'	f	s'	s	U	C_D
	in	-	in	in	in/sec	-
44	0.110	0.2855	0.72	2.135	11.26	0.414
	0.120	0.3115	0.80	2.184	11.50	0.397
45	0.155	0.342	1.05	2.615	13.75	0.389
	0.140	0.309	0.95	2.620	13.80	0.3875
46	0.165	0.319	0.735	1.786	9.40	0.377
	0.165	0.319	0.720	1.740	9.16	0.396
47	0.20	0.3472	1.74	3.655	19.22	0.38
	0.185	0.321	1.35	3.63	19.10	0.385
41	0.20	0.3145	1.03	2.623	13.80	0.398
	0.215	0.342	1.12	2.645	13.92	0.39
42	0.21	0.3295	1.07	2.61	13.73	0.399
	0.205	0.3215	1.06	2.66	14.00	0.384
43	0.205	0.3191	1.05	2.648	13.94	0.3985
39	0.24	0.317	1.39	3.63	19.10	0.409
	0.245	0.3235	1.45	3.731	19.62	0.387
40	0.25	0.331	1.52	3.84	20.20	0.399
	0.25	0.331	1.48	3.715	19.56	0.426
48	0.24	0.331	1.47	3.72	19.54	0.403
	0.25	0.345	1.52	3.68	19.38	0.411
49	0.23	0.3172	1.40	3.69	19.40	0.413
	0.23	0.3172	1.40	3.69	19.40	0.413
50	0.23	0.3172	1.39	3.66	19.25	0.416

T A B L E 5 (CONTINUED)

Sphere No.	d' in	f -	s' in	s in	U in/sec	C_D -
50	0.24		1.48			
51	0.23		1.39			
	0.23		1.45			
52	0.24	0.331	1.46	3.685	19.40	0.406
	0.24		1.46			
53	0.24		1.45			0.404
54	0.23	0.3172	1.38	3.63	19.10	0.423
	0.225	0.31	1.36	3.66	19.25	0.416
55	0.225	0.31	1.34	3.60	18.93	0.425
	0.23	0.3172	1.39	3.66	19.25	0.413
56	0.238	0.328	1.44	3.73	19.62	0.392

TABLE 6

Sphere No.	d in	λ min/d -	λav/d -	λmax/d -	ρ_s/ρ_w -	$\frac{(\lambda/d)max}{(\lambda/d)_{av.}}$ %
44	0.385	15.3	17.8	20.5	0.735	15.17
45	0.453	13.0	15.95	19.0	0.685	19.13
46	0.517	26.2	26.4	27.4	0.875	2.62
47	0.576	11.8	14.15	14.6	0.526	3.18
41	0.629	11.5	15.0	18.5	0.766	23.32
42	0.376	15.7	18.6	20.7	0.770	15.60
43	0.642	16.2	18.45	19.5	0.765	12.20
39	0.757	13.86	14.72	15.6	0.618	6.51
40	0.755	12.24	12.75	16.16	0.582	4.00
48 to 58	0.725	10.62	11.3	12.7	0.59	12.39

$$\left(\frac{\Delta\ (\lambda/d)_{max}}{(\lambda/d)_{av.}} \right)_{average} = 11.41\ \%$$

T A B L E 7.

Sphere No.	d in	A_{max} in	ρ_s/ρ_w -	A/d -	$1-\rho_s/\rho_w$ -
44	0.385	0.6	0.735	1.560	0.265
45	0.453	0.7	0.6845	1.543	0.3155
46	0.517	0.423	0.875	0.818	0.125
47	0.576	1.0	0.526	1.734	0.474
41	0.629	1.07	0.7655	1.701	0.2345
42	0.637	0.642	0.770	1.009	0.230
43	0.642	0.81	0.765	1.260	0.235
39	0.757	0.8	0.618	1.057	0.382
40	0.755	0.8	0.582	1.06	0.418
48 to 58	0.725	0.8	0.59	1.103	0.41

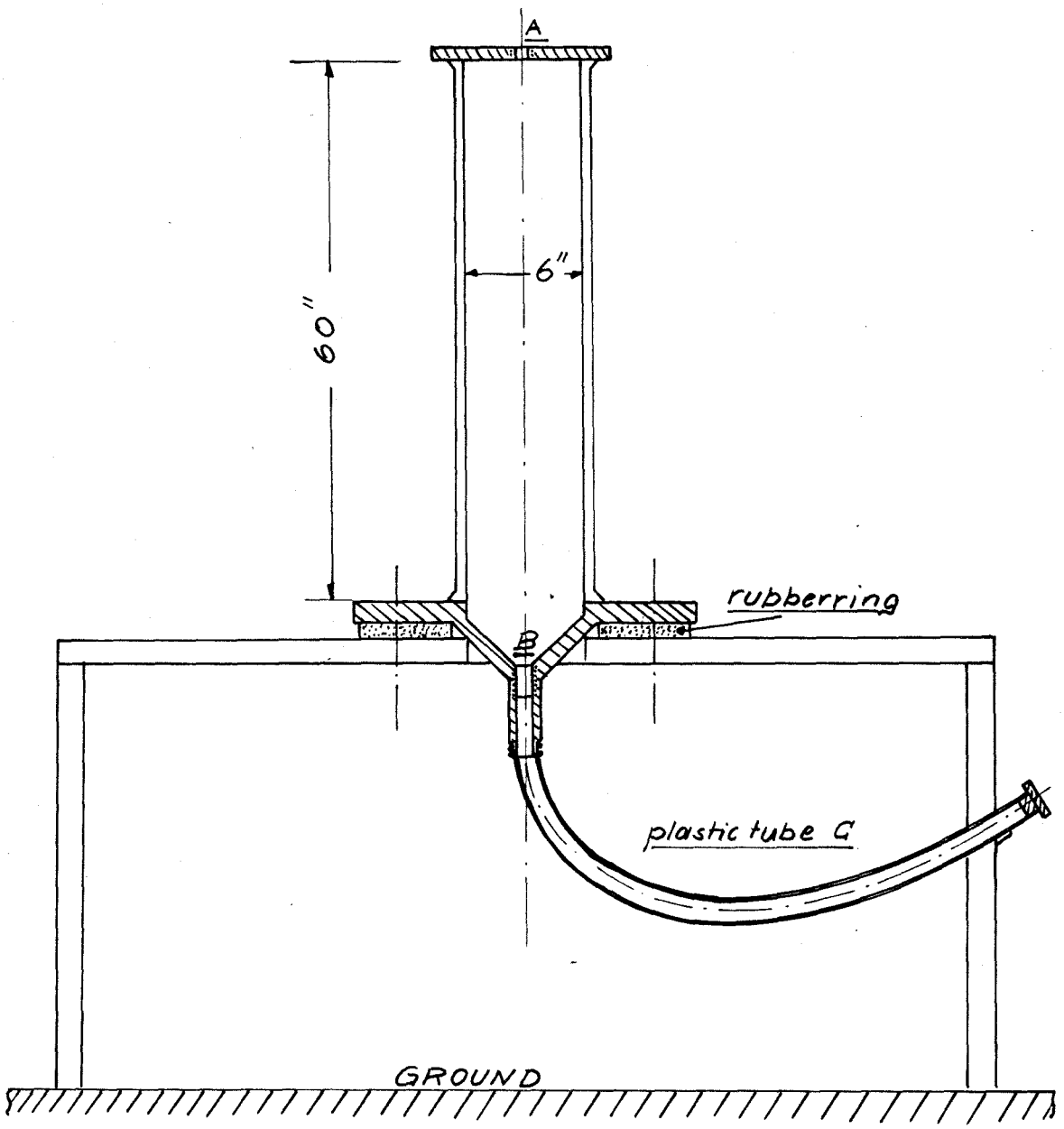

figure 1. TEST SET-UP

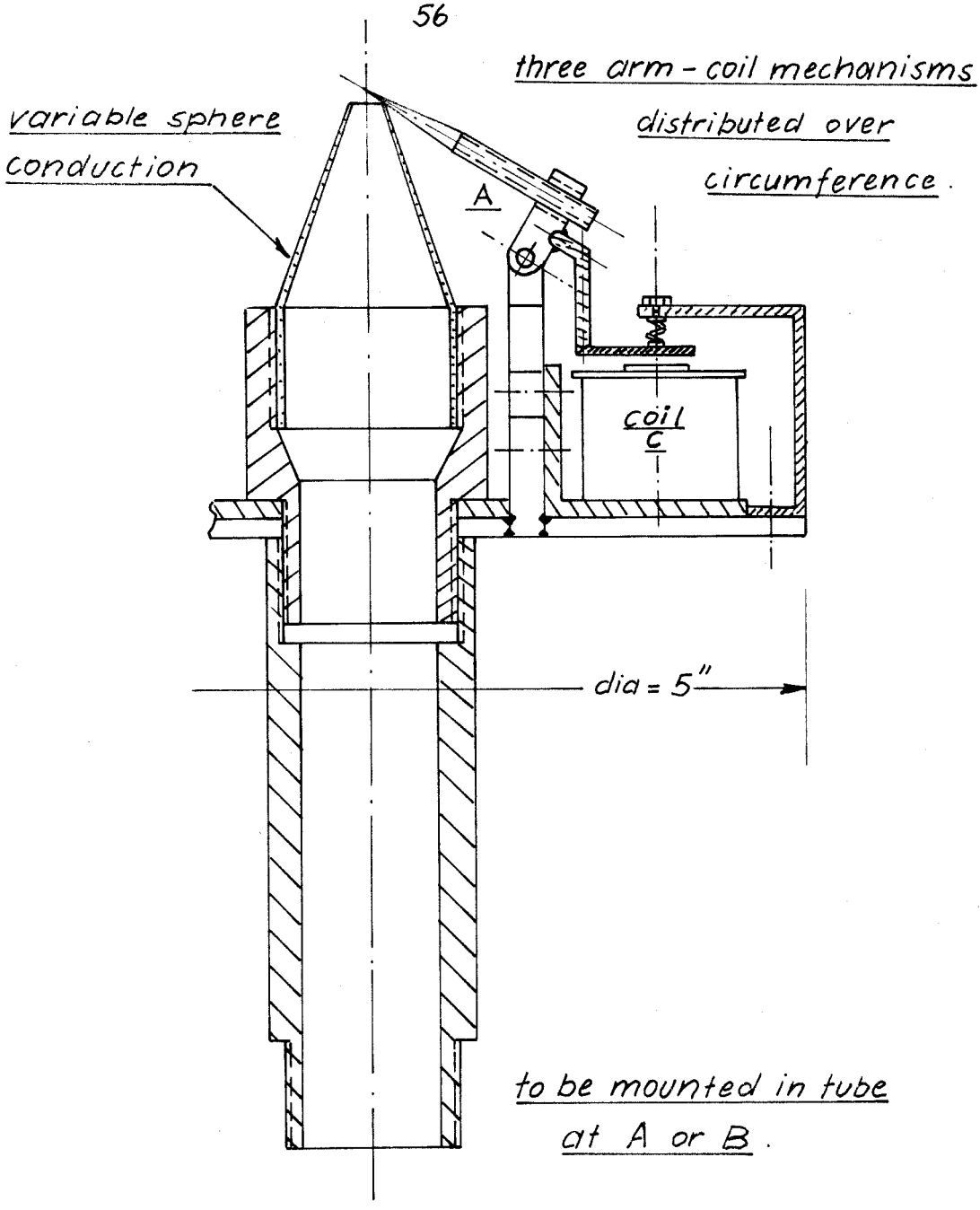

figure 2. SPHERE RELEASE

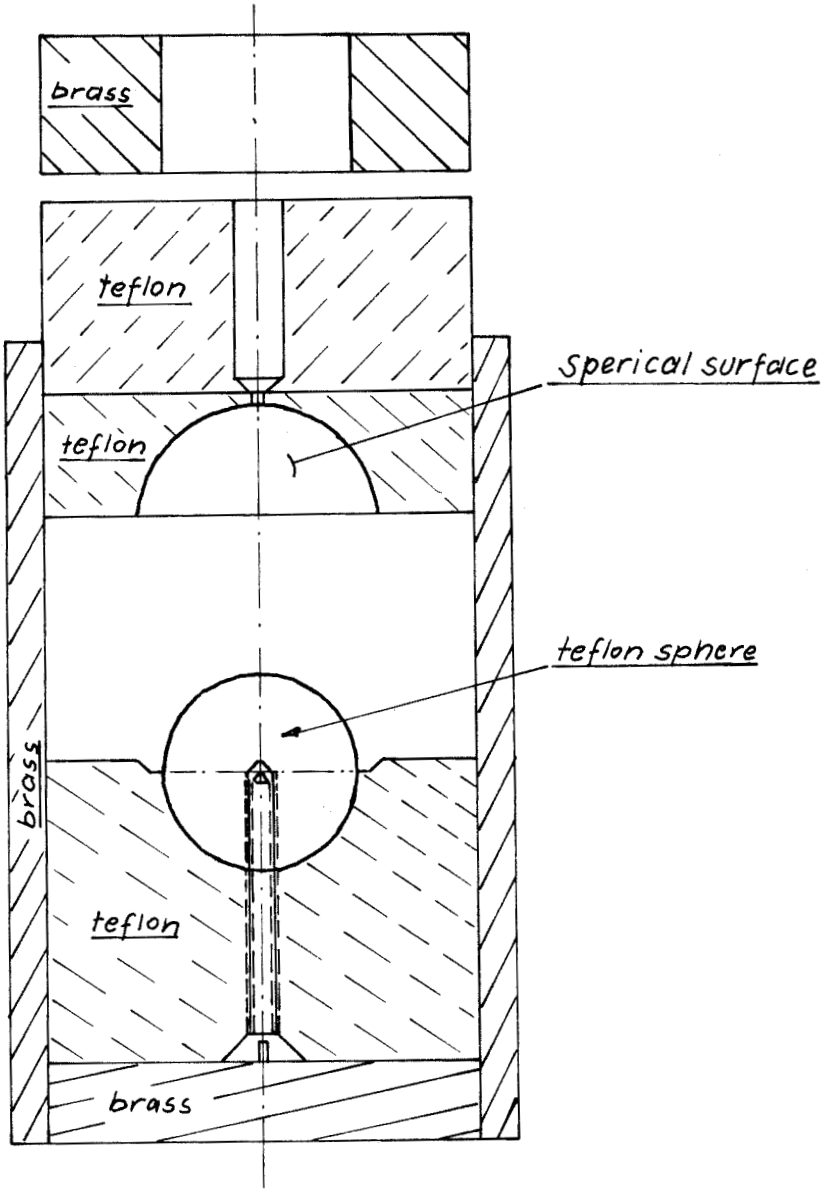

figure 3. SPHERE MOLD

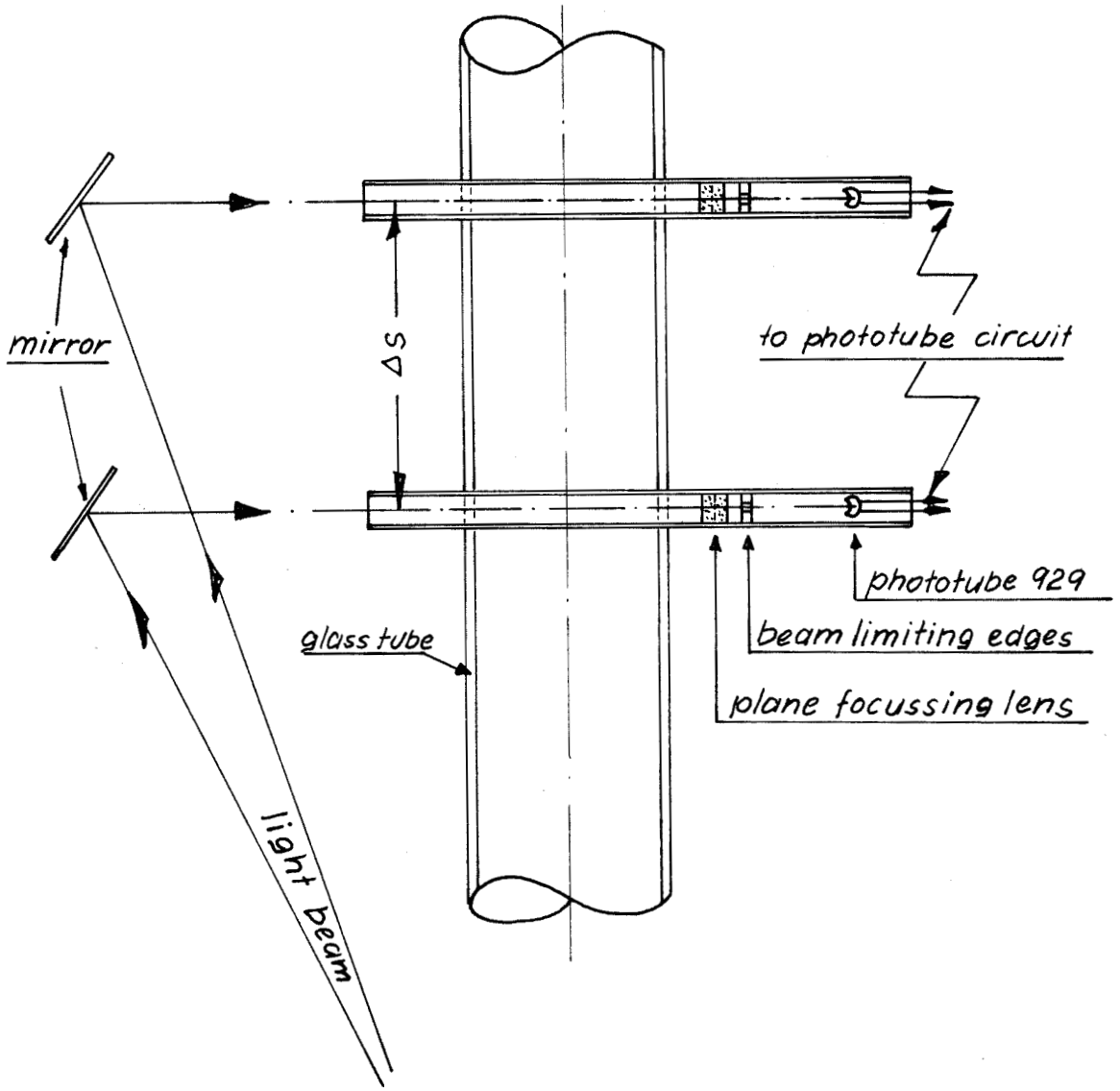

figure 4. PHOTOTUBE TIMING DEVICE
(schematic)

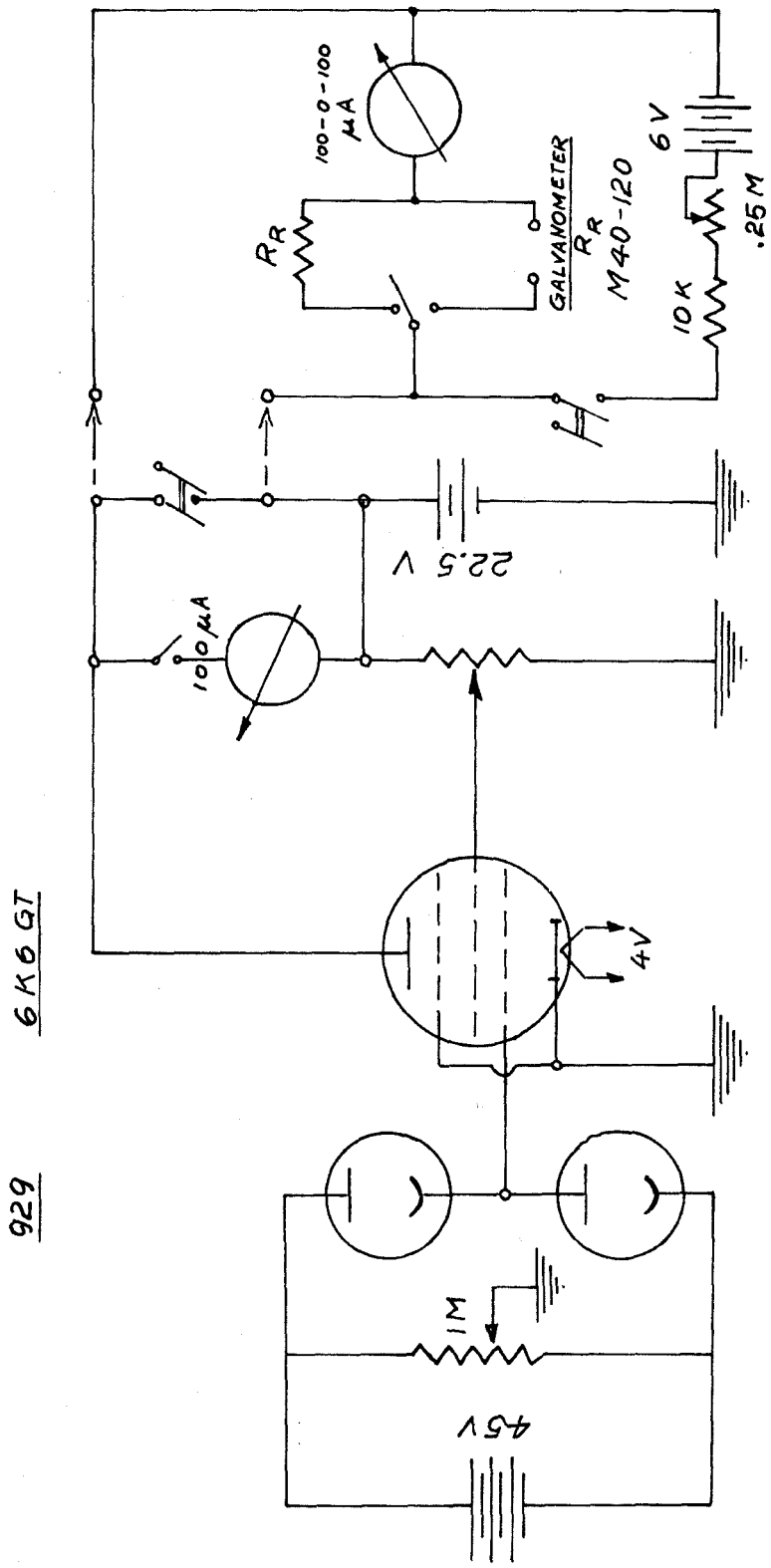

figure 4a. PHOTOTUBE CIRCUIT AND ZERO-BALANCING OUTPUT CIRCUIT

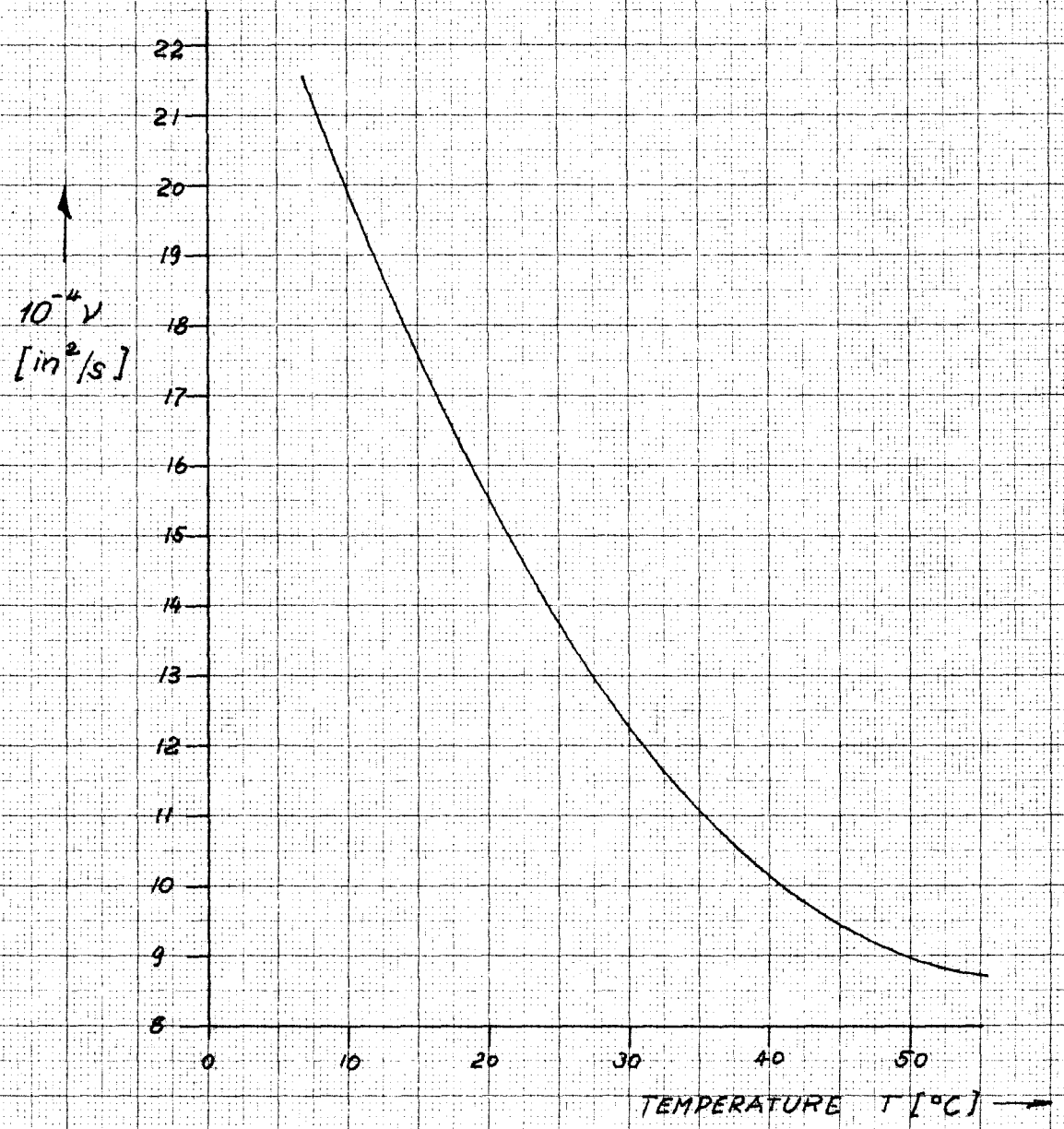

figure 5. KINEMATIC VISCOSITY OF WATER

$\nu_w = \nu(T)$ from (3)

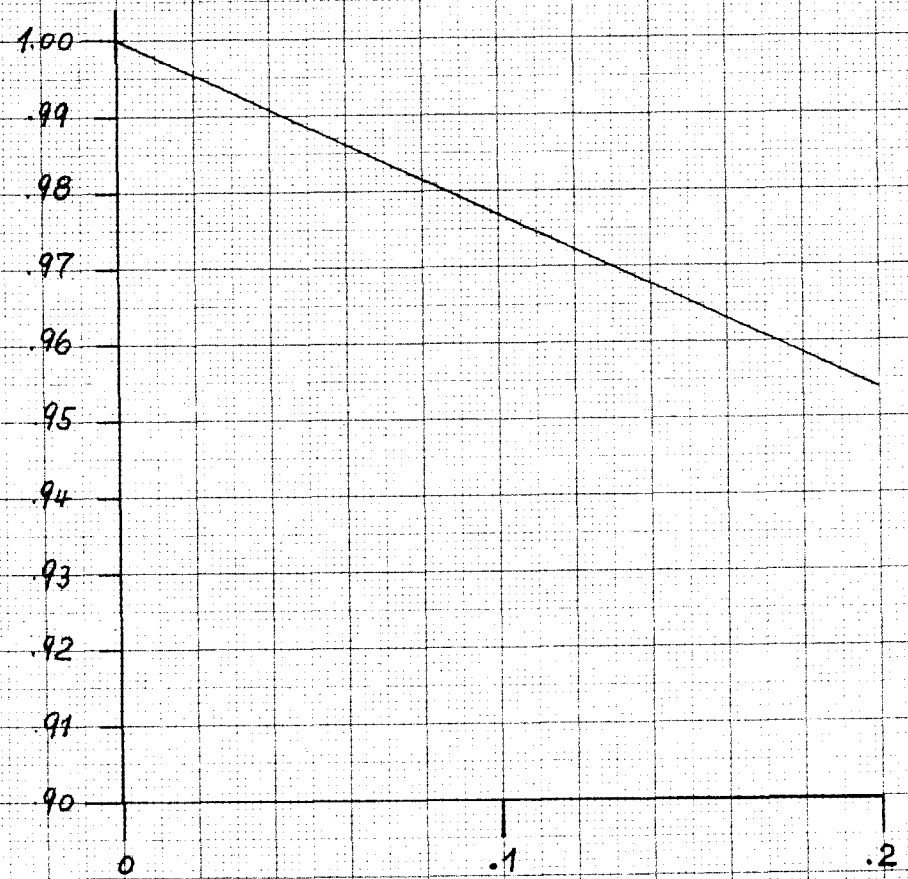

figure 6. WALL CORRECTION FACTOR FOR WATER

$K_W = U/U_o = 1 - 0.23\ d/D$ from (4)

U_o = VELOCITY IN UNBOUNDED WATER $d/D = 0$, $D = \infty$

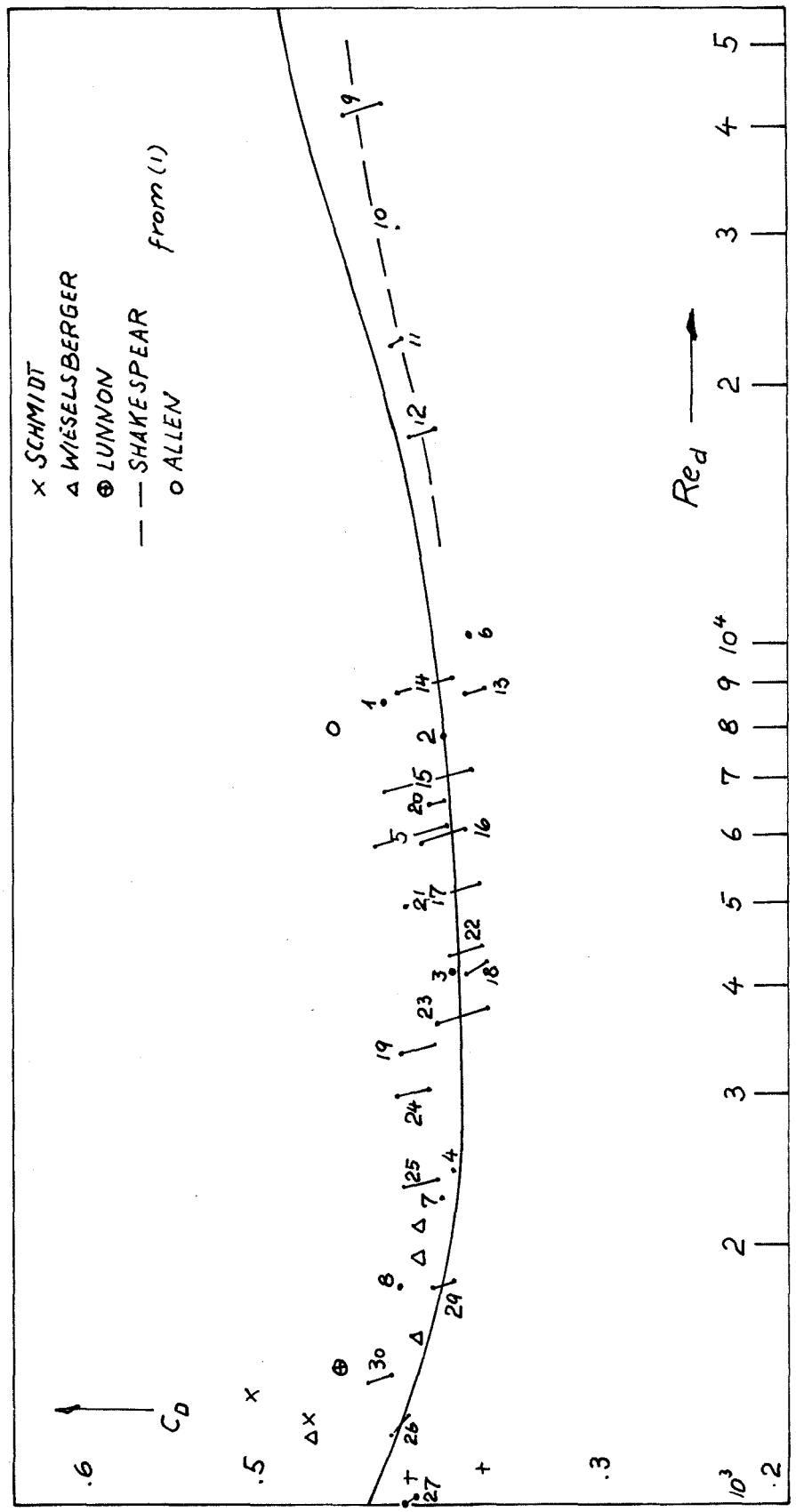

figure 7. DRAGCOEFFICIENT OF FREE-FALLING SPHERES

THE NUMBERS REFER TO TABLE 1

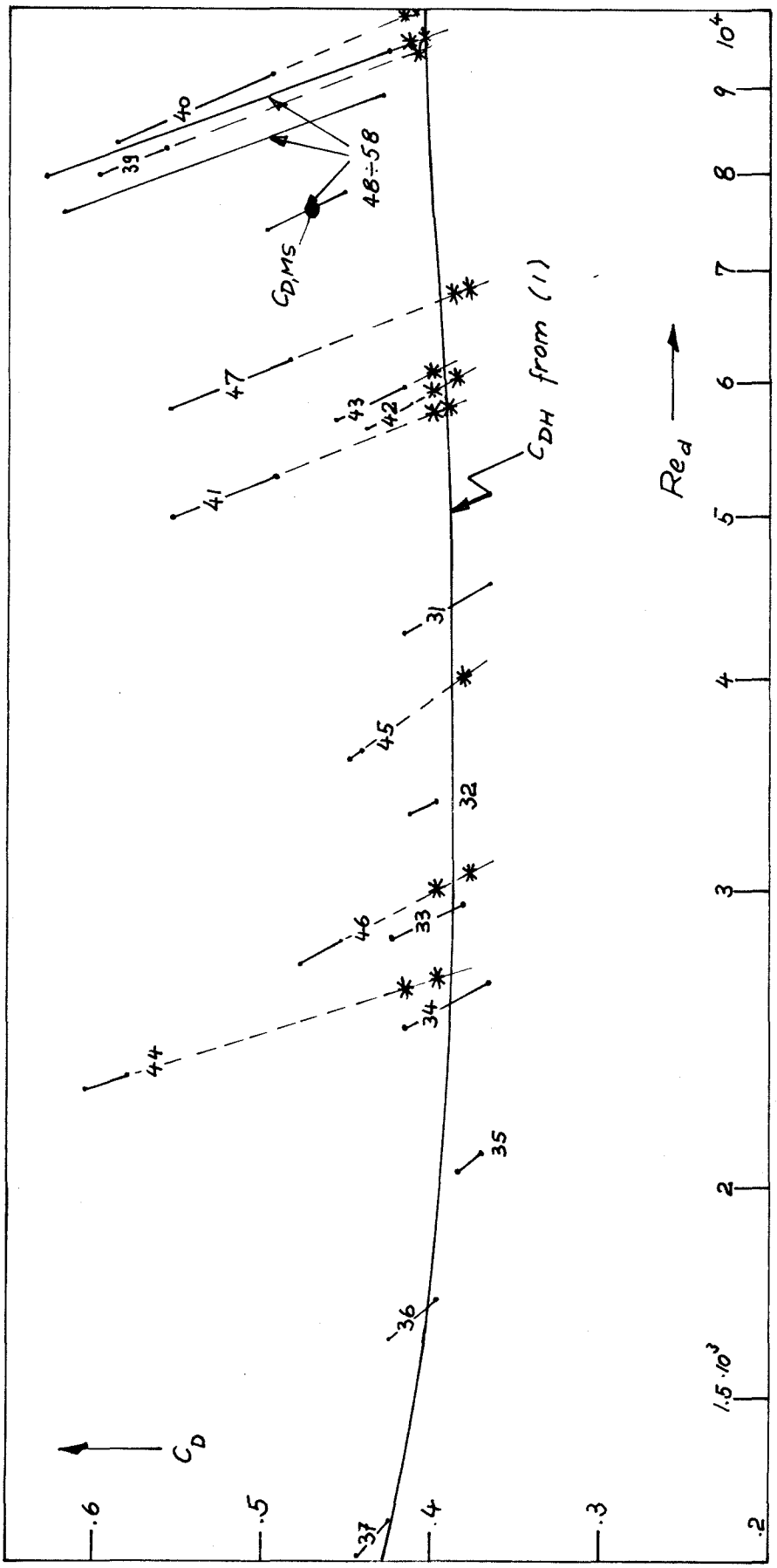

figure 8. DRAGCOEFFICIENTS OF RISING SPHERES

THE NUMBERS REFER TO TABLE 2

—•— FROM TABLE 4 * FROM TABLE 6

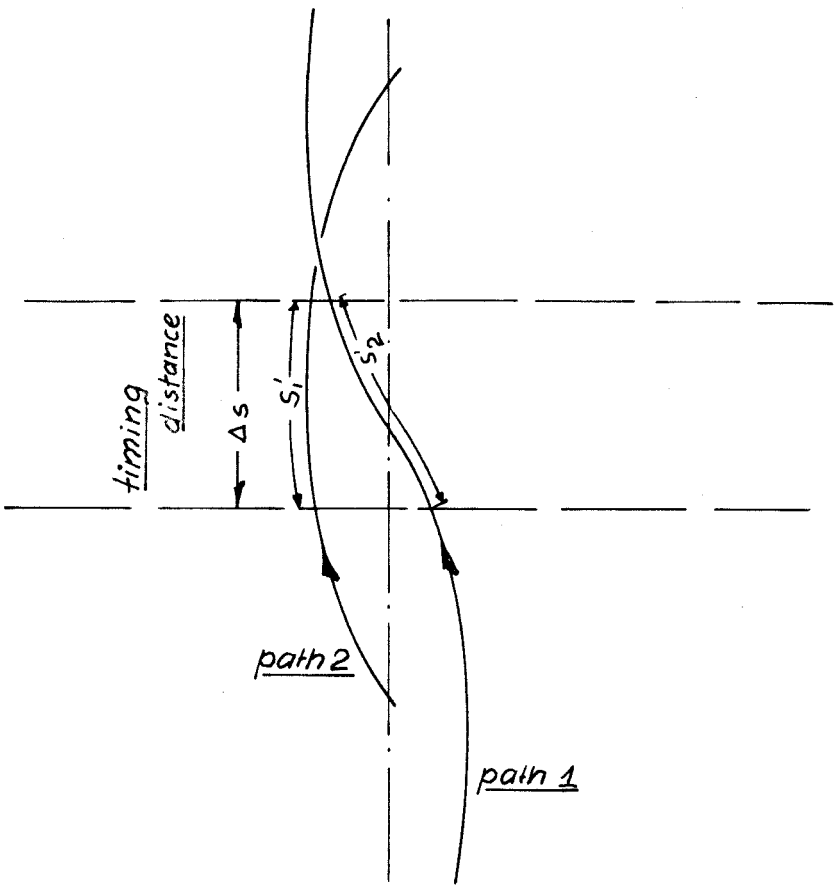

figure 9. POSITION OF WAVY SPHERE PATH

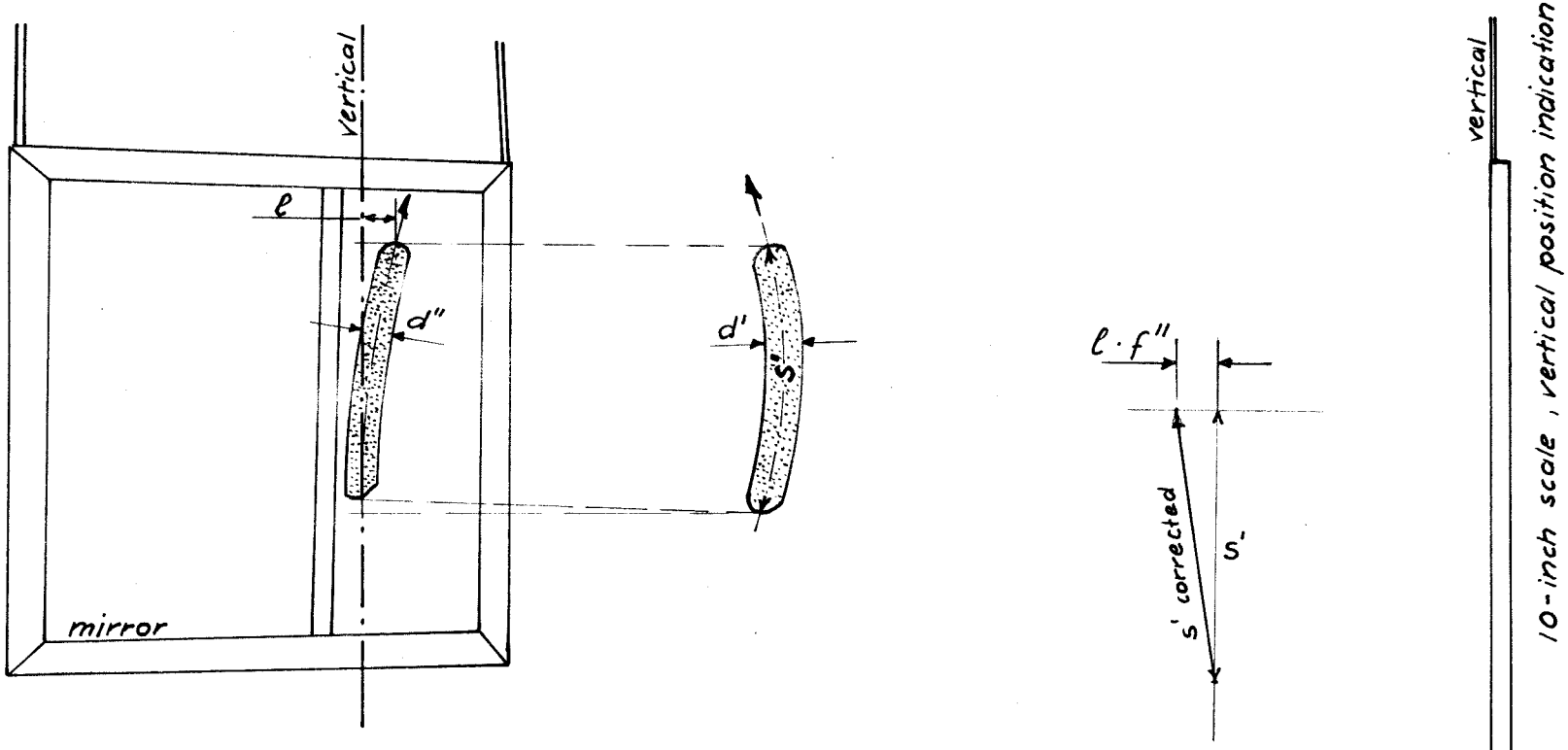

$d'' = .16$ inch $\qquad d' = .20$ inch $\qquad \ell = .175$ inch

$d = 0.576$ inch $\qquad f'' = \frac{d'}{d''} = 1.25$

sphere № 47

$s'_{uc} = 1.45$ inch

$s'_{corr} = 1.47$ inch $= s'$

figure 10. TYPICAL PHOTOGRAPH FOR DETERMINATION OF LOCAL SPHERE-VELOCITY

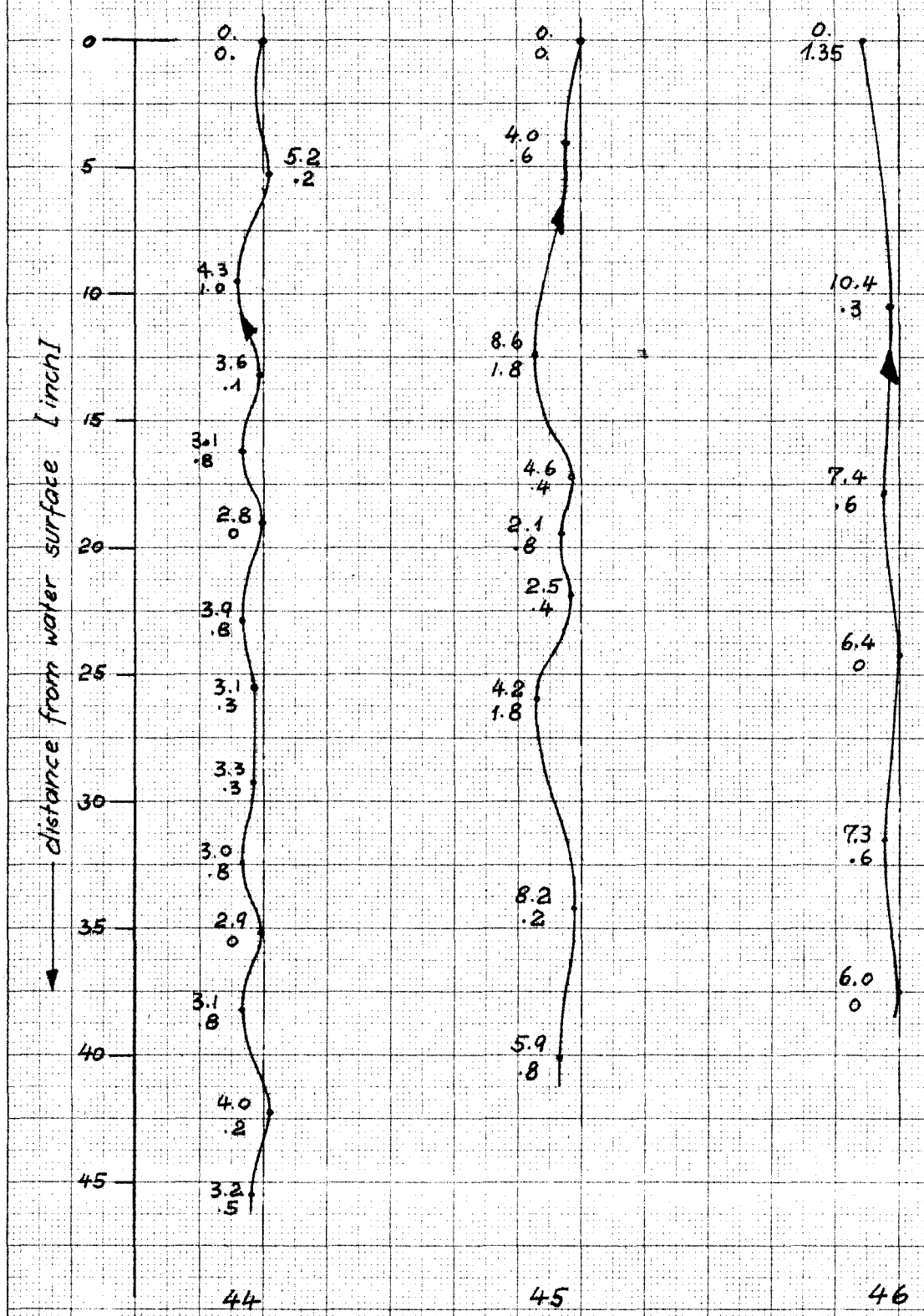

figure IV. SPHERE PATH

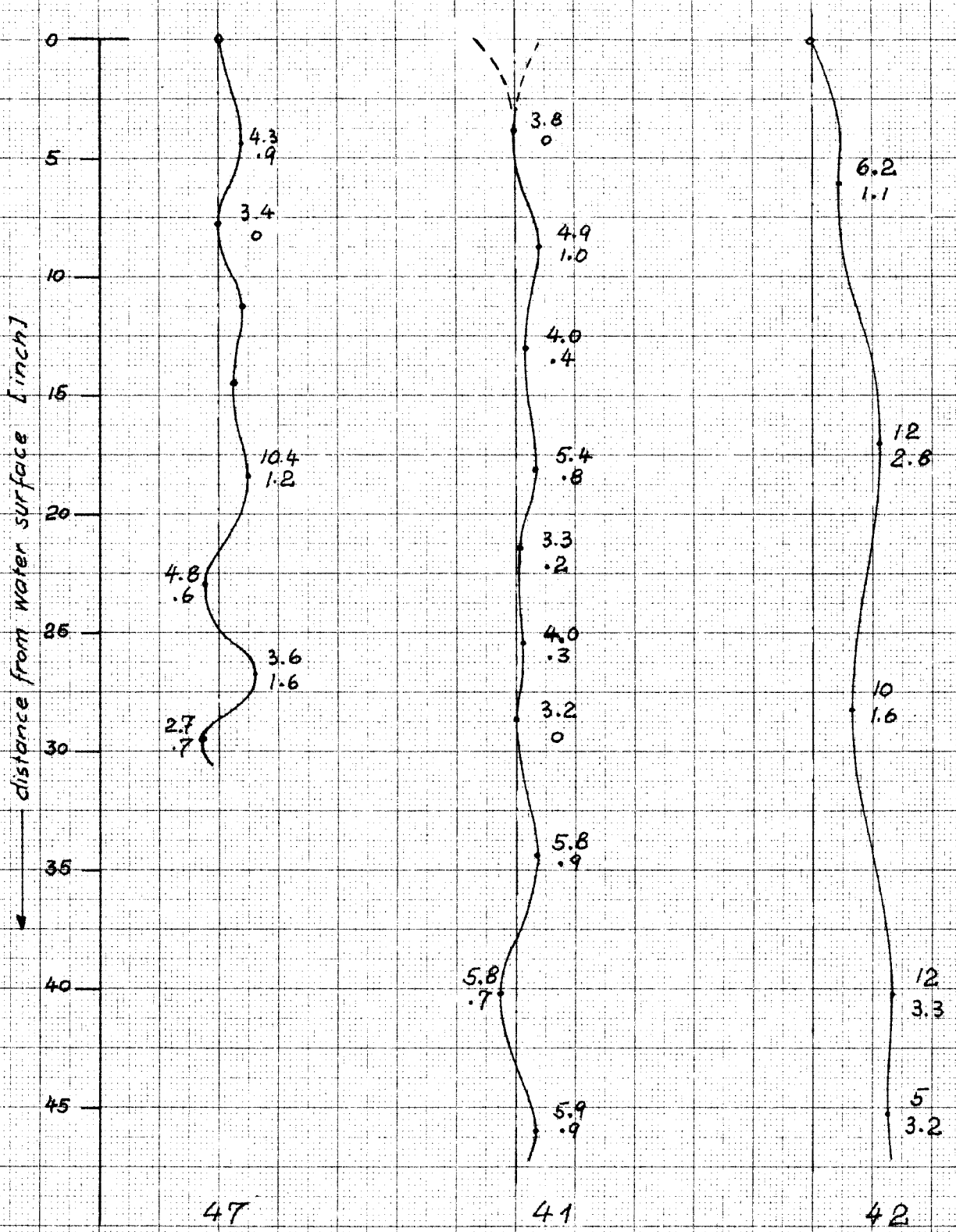

figure 12. SPHERE PATH

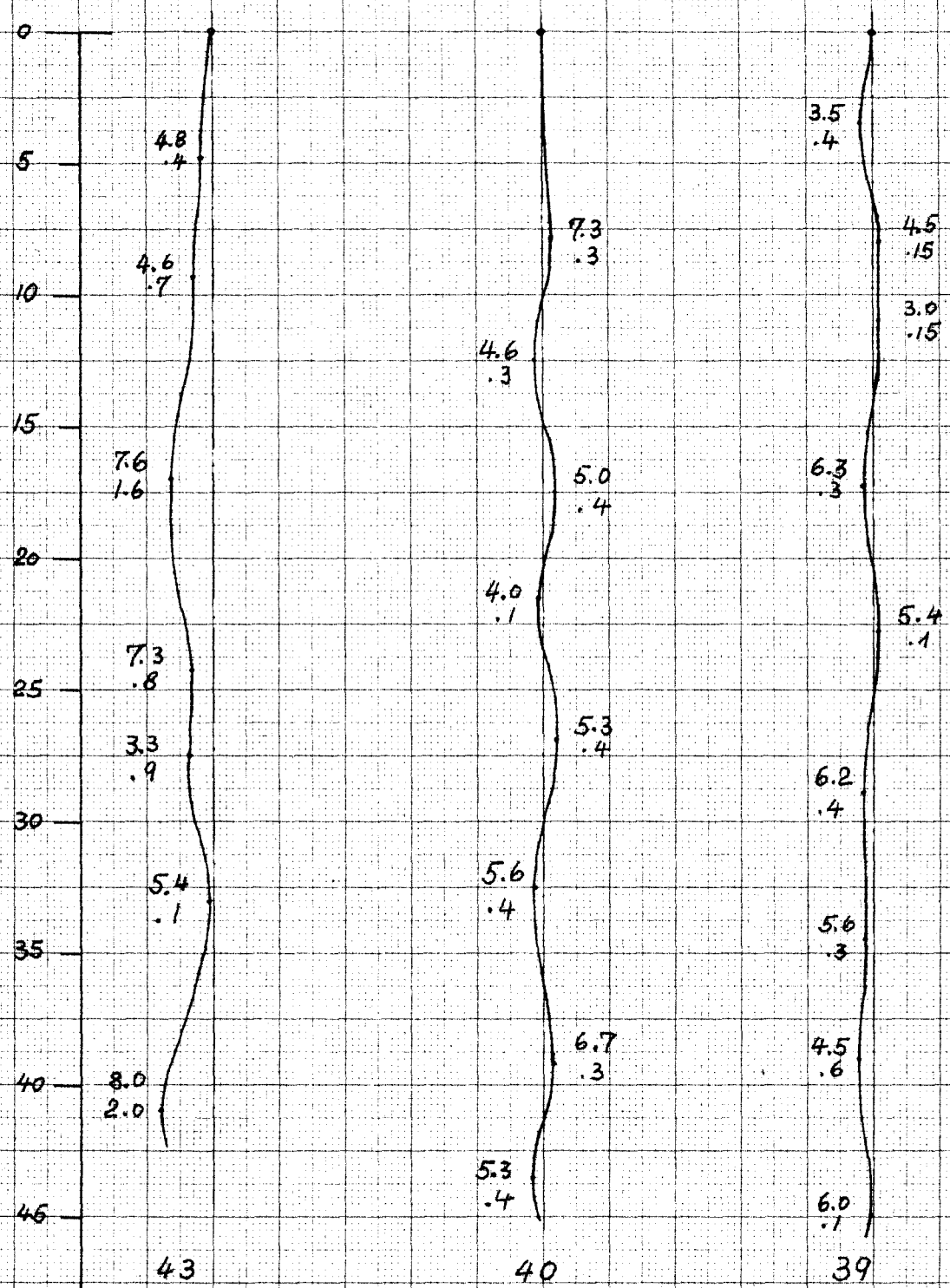

figure 13. SPHERE PATH

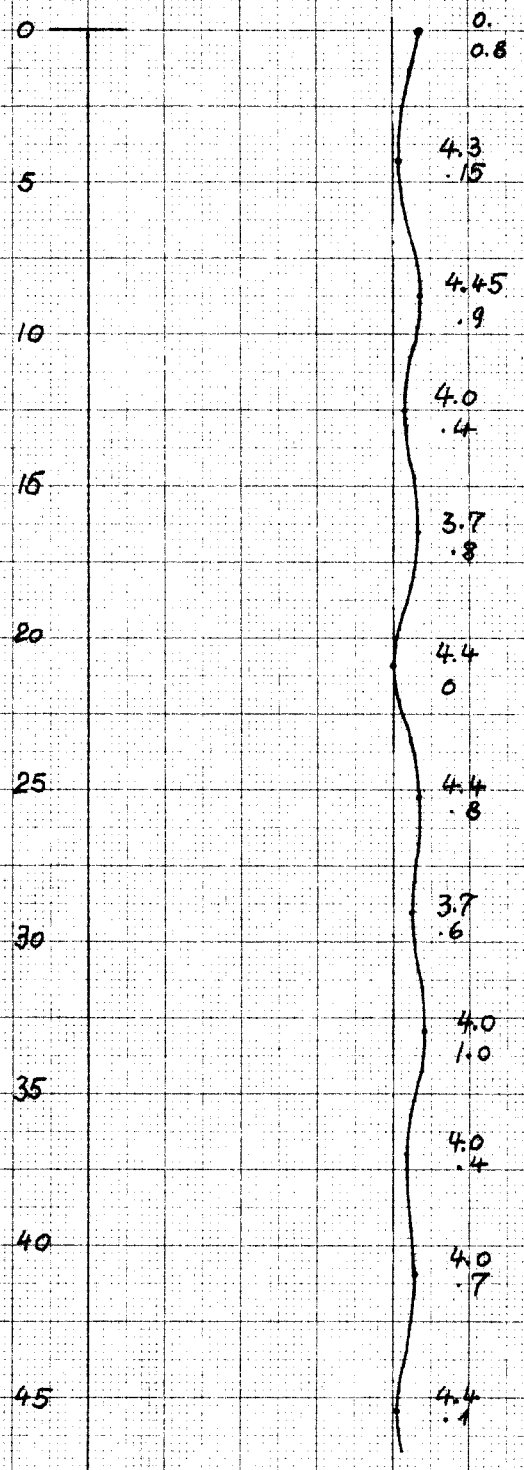

48 to 58

figure 14. SPHERE PATH

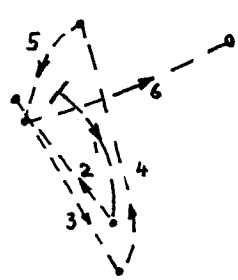

44

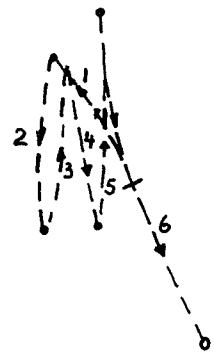

45

46

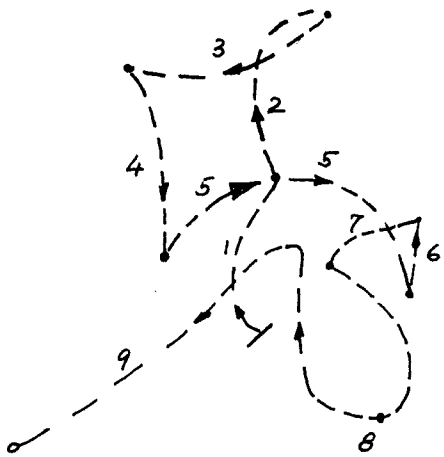

47

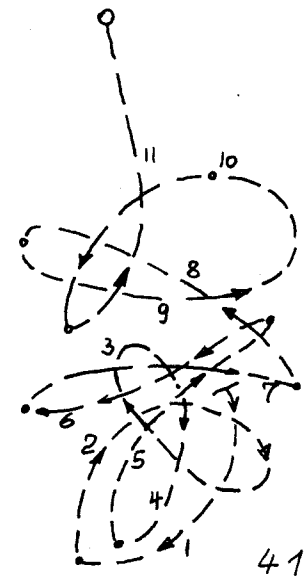

41

figure 15. AMPLITUDE OF SPHERE PATH

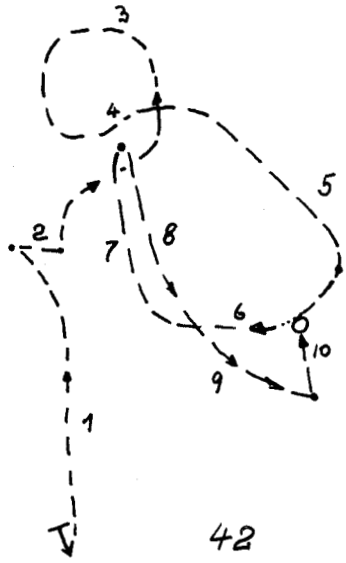

42

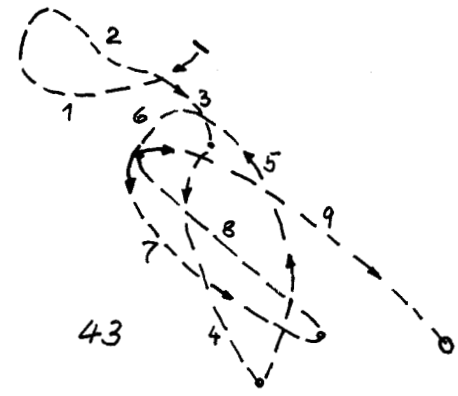

43

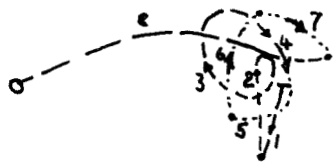

40

39

figure 16 . AMPLITUDE OF SPHERE PATH

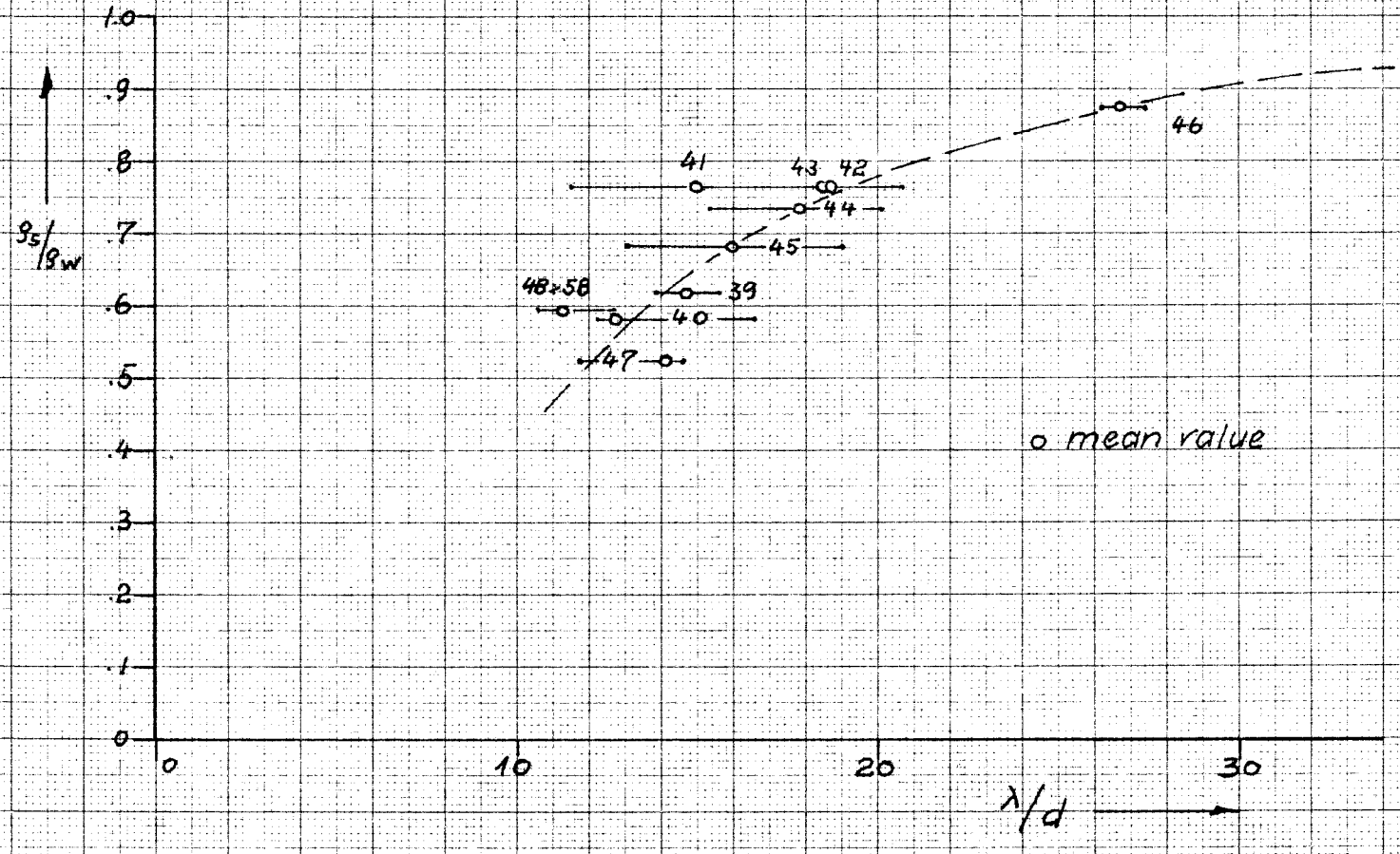

figure 17. WAVELENGTH λ AS FUNCTION OF DENSITY RATIO ρ_s/ρ_w

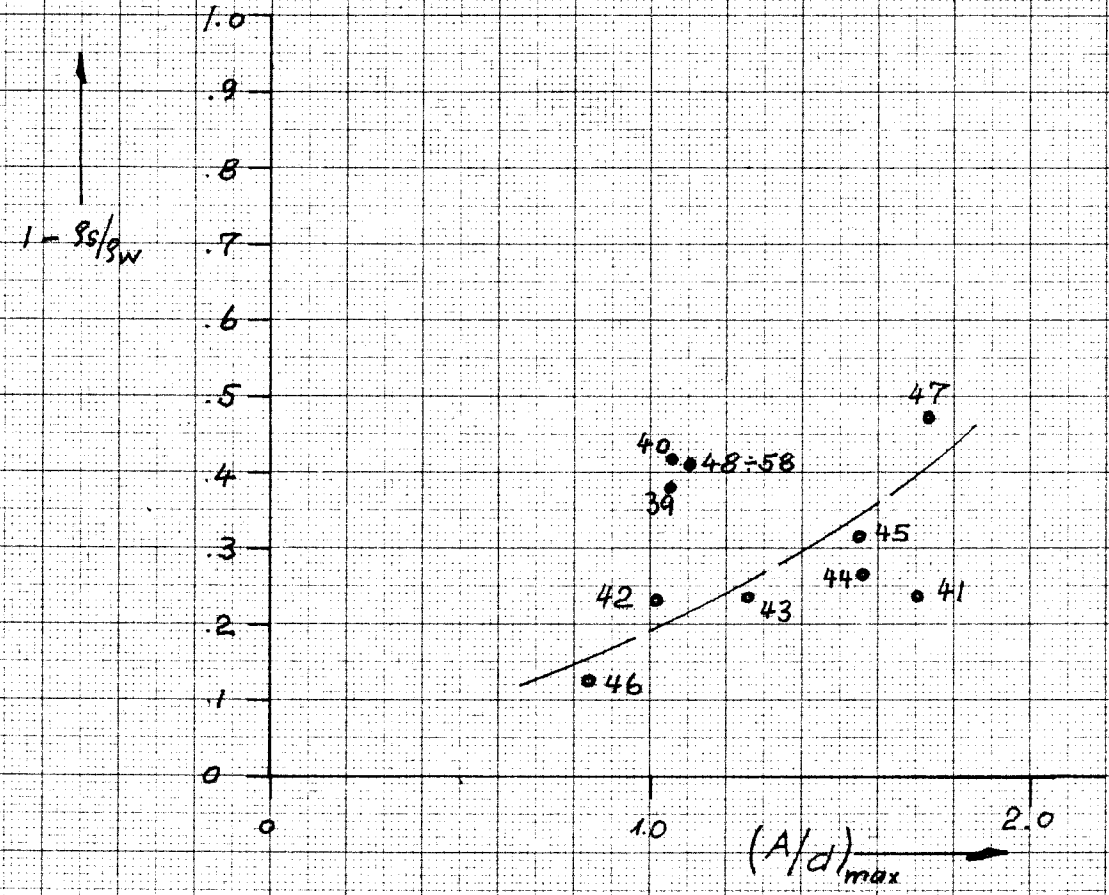

figure 18. AMPLITUDE A AS FUNCTION OF DENSITY RATIO ρ_s/ρ_w

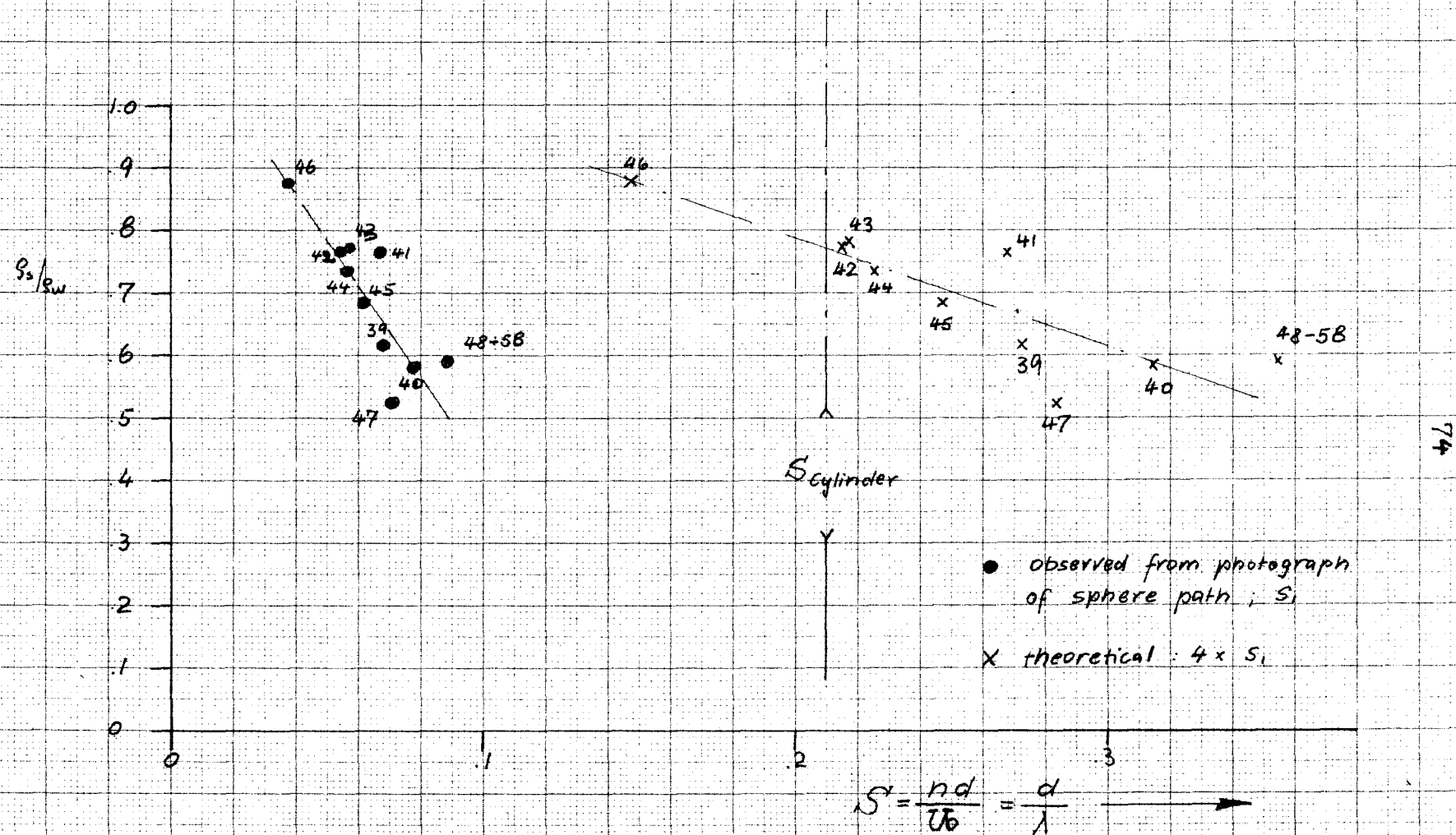

74

figure 19. STROUHAL NUMBER AS FUNCTION OF ρ_s/ρ_w.

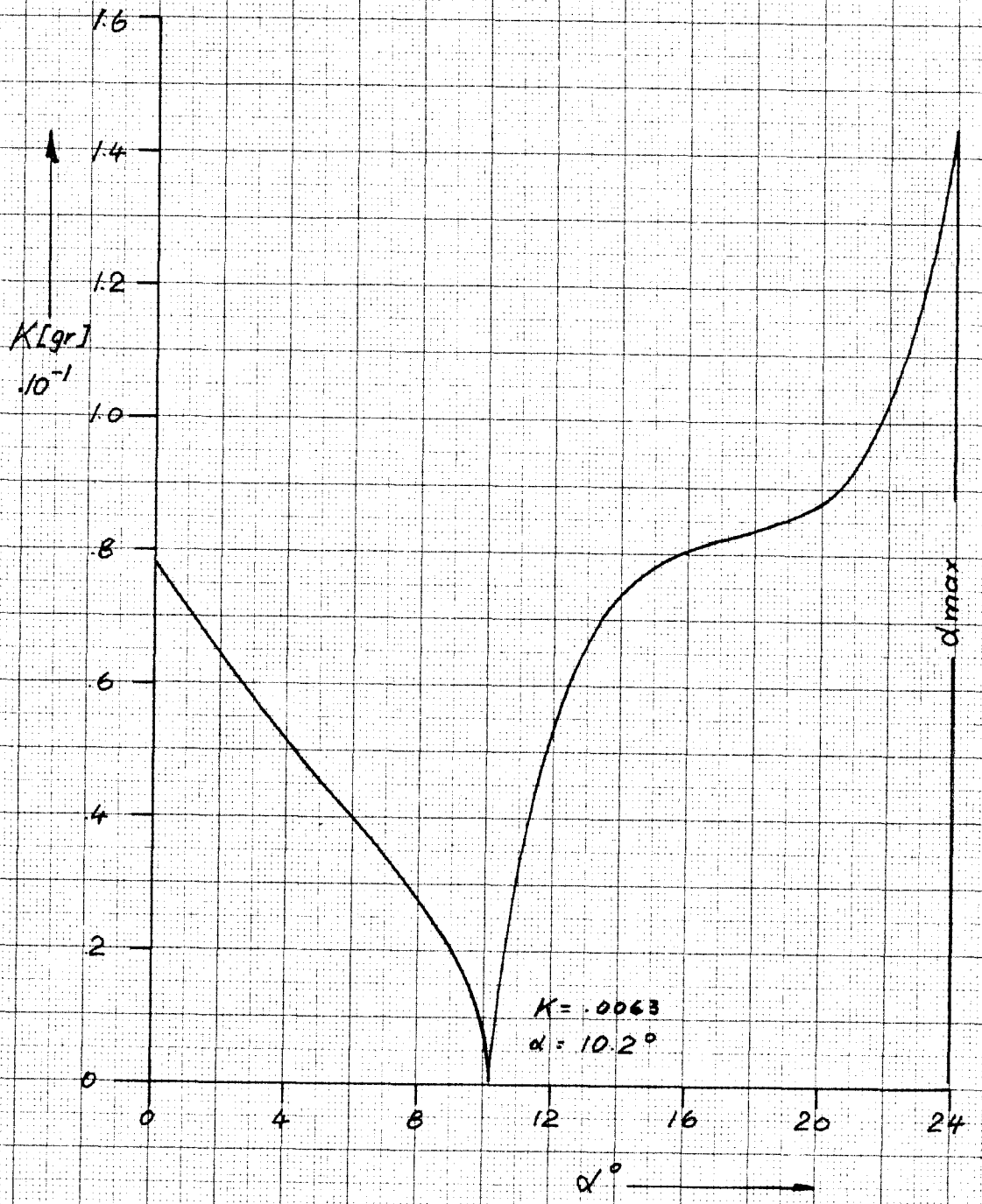

figure 20. PRESSURE FORCE $K = K(\alpha)$

for SPHERE NO. 47

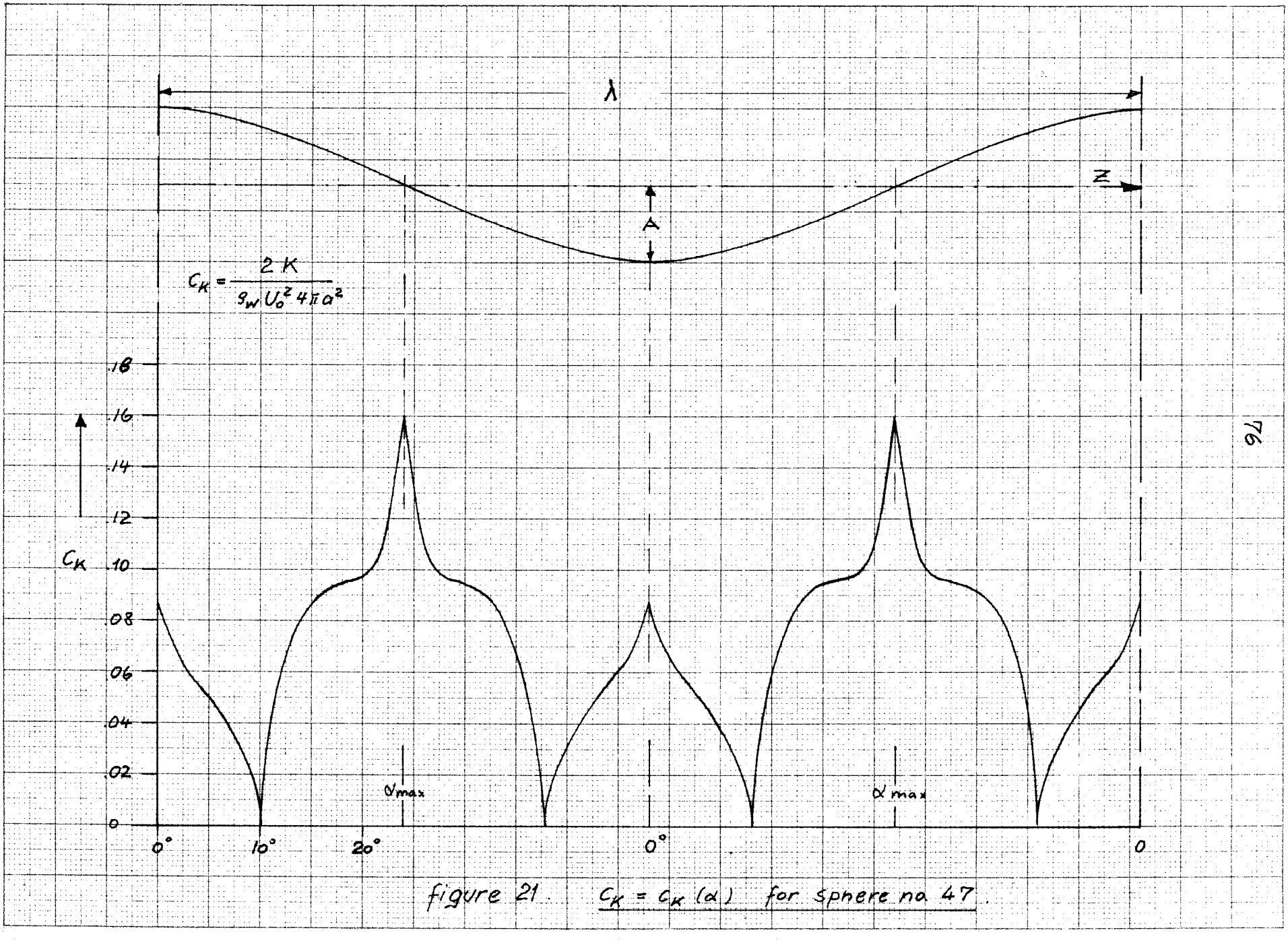

figure 21. $C_K = C_K(\alpha)$ for sphere no 47.